and cholangiocytes (bile duct cells). The common progenitors of hepatocytes and cholangiocytes are derived from hepatoblasts in the hepatic endoderm. The hepatic endoderm arises from the foregut endoderm that interacts with adjacent tissues, such as the cardiac mesoderm and septum transversum mesenchyme (Douarin, 1975; Grapin-Botton and Melton, 2000; Tam et al., 2003; Zaret, 2001). The vasculature is another important component of the liver. Angioblasts, which are endothelial cell precursors, accumulate around the liver bud and become interspersed with the hepatoblasts (Matsumoto et al., 2001).

Regulatory genes that are crucial for liver formation have been isolated in mice and confirmed by reverse genetics (see Zaret, 2002 for a review). For instance, we have shown using SEK1 or MKK7-deficient mice that two stress-signaling kinases, SEK1 (also called MKK4) and MKK7, play crucial roles in hepatoblast proliferation and survival (Nishina et al., 1999; Wada et al., 2004; Watanabe et al., 2002). Although a reverse genetic approach is powerful in characterizing functions of known genes, knowledge of genes, particularly in hepatic bud formation from endoderm, morphogenesis and laterality of the liver, and hemoglobin–bilirubin or lipid metabolism, is still limited. Therefore, identifying mutations affecting these aspects of liver formation and function will uncover genes required for these processes.

Systematic forward genetic screens for mutations affecting embryogenesis have been carried out in zebrafish. Zebrafish embryos are transparent and sustain defects in circulation or hematopoiesis, because oxygen supplied by simple diffusion is sufficient for development and the liver is not the site of embryonic hematopoiesis (Alexander and Stainier, 1999). These characteristics of zebrafish have enabled the study of genes involved in the development of endoderm, cardiovascular and hematopoietic systems. Zebrafish mutants with impaired endoderm formation, degenerative liver, impaired lipid metabolism in the intestine and hepatobiliary system, have been identified (Chen et al., 1996; Farber et al., 2001; Pack et al., 1996; Schier et al., 1996, 1997; Zhang et al., 1998). Furthermore, the availability of transgenic lines expressing GFP throughout the digestive system allows direct observation of the endoderm and digestive organ formation in living embryos (Field et al., 2003; Ober et al., 2003). However, genes identifiable in a single model organism by the mutational approach are limited due to a functional overlap of genes in vertebrates.

Medaka is evolutionally distant from zebrafish and interspecies differences in the functional overlap of genes allow identification of mutations as yet unidentified in zebrafish. The liver and gall bladder are more conspicuous in living embryos in Medaka than in zebrafish. Medaka has a smaller genome size (half that of zebrafish, and only double that of Fugu), inbred strains are available, and a wide range of growth temperatures facilitates identification of temperature sensitive mutations.

Taking advantage of these attributes of Medaka, we have carried out a mutagenesis screen, using multiple assays to detect defects in various aspects of the development of a functional liver. These include not only morphological assays, but also those of the functions related to the liver, such as hemoglobin–bile and lipid metabolism. In this report, we present the initial characterization of mutations isolated in the screen, ranging from those affecting endoderm formation to those affecting liver physiology in Medaka.

2. Results

2.1. Designing of mutant screening based on multiple criteria

2.1.1. Morphological screening

We carried out the morphological screen of the liver by inspecting live embryos when the liver became discernible from 4 days post-fertilization (dpf, stage (st.) 32) at 28 °C and the gall bladder became prominent at approximately 120 h post-fertilization (hpf, st. 36). The lateral views of wild-type embryos and livers at st. 32 and 36 are shown in Fig. 1A–C. The liver, gall bladder, and blood vessel from the liver connected to the Cuvierian duct developing on the left side of the embryo were observed (Fig. 1B,C).

To analyze the time course of liver development, we carried out in situ hybridization between st. 21 and 39 using endoderm-specific markers, *foxA3* and *gata6* (Fig. 1D–P). The hepatic bud formed from the endoderm rod in wild-type Medaka at st. 25 (Fig. 1H,I). At st. 27 the liver began to enlarge and the swim bladder appeared from the gut tube and began to enlarge (Fig. 1J–P, arrowheads and asterisks indicate the liver and swim bladder, respectively). *foxA3* was also expressed in the pharynx, but unlike in zebrafish, *foxA3* was not expressed in the pancreas in Medaka (data not shown). On the other hand, the expression of *gata6* was restricted to the liver from st. 25 to 31 (Fig. 1I,K,M). Soon after at st. 31, we screened live embryos. No expression of *gata6* was detected in the liver at st. 34 (Fig. 1O). In zebrafish, *gata6* is expressed in the liver and gut. Thus, the expression pattern of *gata6* in Medaka is different from that in zebrafish.

Considering the relatively late development of the liver in embryogenesis, care was taken to avoid isolating mutants showing a general retardation of development. Mutants with altered liver morphologies, such as the size, shape, and laterality of livers, were screened first at st. 32 and confirmed at st. 36 when the liver and gall bladder became larger in wild-type embryos.

2.1.2. Screening of gall bladder color

Based on the assumption that impaired bile metabolism in the liver results in an abnormal color of bile, we inspected

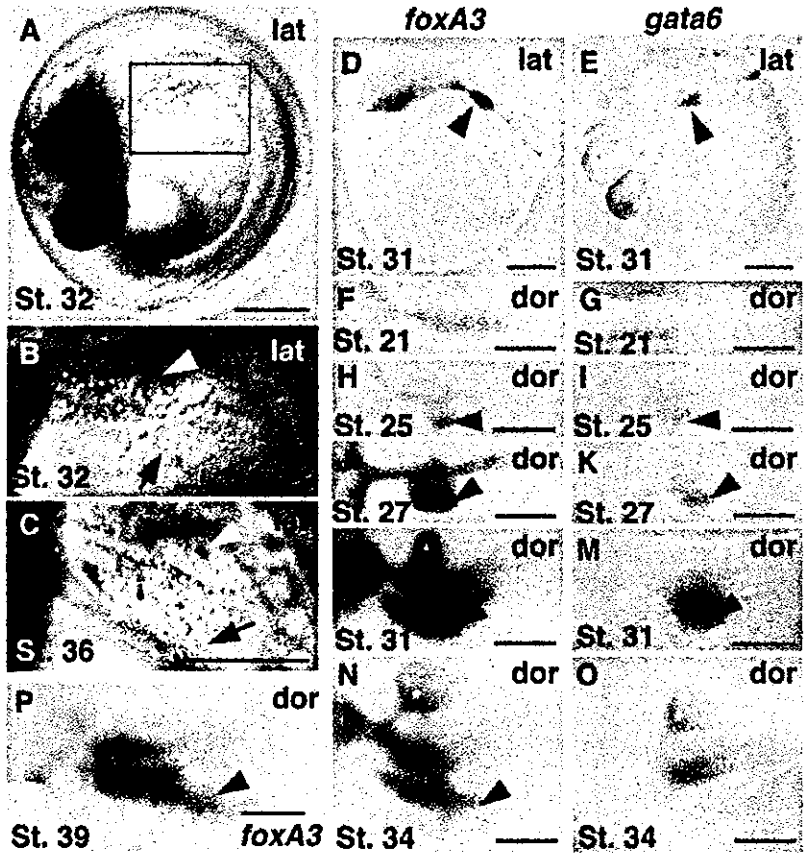

Fig. 1. Liver development in Medaka. Live (A–C) and fixed wild-type embryos stained by in situ hybridization using the *foxA3* (D, F, H, J, L, N, and P) and *gata6* (E, G, I, K, M, and O) probes. (A–C, D, and E) Lateral view; (F–P) Dorsal view. (A–C) The liver was readily visible from the left side of living embryos at st. 32 (A and B) and st. 36 (C) when screening was carried out; (F and G) st. 21; (H and I) The hepatic bud was formed at st. 25 and subsequently liver growth occurred; (J and K) st. 27; (L and M) st. 31; (N and O) st. 34 and (P) st. 39. White broken line demarcates the liver. White arrowheads and black arrows indicate the gall bladder and the vein of the liver, respectively. Black arrowheads and white asterisks show the hepatic bud and the liver, and the swim bladders, respectively. lat: lateral, dor: dorsal. Scale bars correspond to 200 μm.

color of bile in the gall bladder. Bile in the wild-type embryo at st. 35 was light green. Impaired erythropoiesis was reported to alter bile color in zebrafish (Shafizadeh et al., 2002). To distinguish mutations affecting erythropoiesis from those affecting bile metabolism in the liver, we carried out hemoglobin staining with *o*-dianisidine and in situ hybridization analysis using embryonic globins such as *α-0*, *α-1*, and *β-1 globins*.

2.1.3. Screening using fluorescent phospholipid reporters

We used a fluorescent phospholipid reporter, PED6, to screen for mutations affecting lipid metabolism (Farber et al., 2001).

PED6 is a synthetic substrate for PLA_2 that becomes fluorescent after cleavage in the intestine and its fluorescent PED6 metabolites undergo rapid hepatobiliary transport, labeling the liver before the gall bladder, as shown in Fig. 5C. Embryos administered with PED6 showed intense fluorescence in the gall bladder, liver and intestinal lumen. We screened for embryos showing an impaired accumulation of the fluorescent metabolites of PED6. To exclude mutations affecting the swallowing of PED6, the unquenched form of PED6, BODIPY-FL-C5, was used.

2.1.4. Rescreening for mutations affecting early embryogenesis using the foxA3 probe

In addition to directly screening for liver associated phenotypes, we also screened for mutations affecting endoderm and hepatic bud formations among mutants that were initially identified on the basis of morphological abnormalities (Furutani-Seiki et al., 2004). To this end, we carried out in situ hybridization using *foxA3* at st. 28 (Fig. 1J).

2.2. Mutations affecting formation and function of the liver isolated by the multi-assay screen

By screening 210 F2 families, we have isolated 19 mutations. Since all of the mutations were zygotic recessive mutations, mutants refer to homozygotes of these mutations in this report. These mutations were classified into the following five phenotypic groups and features of these mutations were summarized in Table 1.

2.2.1. Mutations affecting liver morphogenesis

Mutations in four genes, *kakurembo* (*kak*), *hiohgi* (*hio*), *origami* (*ora*) and *kamifusen* (*kam*) affect liver morphology.

In live *kak* embryos at st. 34, the liver was not clearly discernible at the position where it should be formed and the gall bladder was dislocated anteriorly (Fig. 2A,B). In *kak* mutant embryos at st. 24, the expression level of *gata6* in the liver markedly reduced, while that of *cardiac myosin light chain* (*mlc*) in the heart was unaltered (Fig. 2G,H). In *kak* mutant embryos at st. 34, the expression level of *foxA3* was also greatly reduced (Fig. 2I,J). Since liver budding appeared to occur in *kak* mutants, *kak* may be required for the growth or maintenance of the liver. The gut tube was undulated at st. 36 (data not shown) without affecting the epithelial structure of the gut tube (Fig. 2N,O,Q,R).

In *hio* mutant embryos at st. 36 and at later stages, the liver was small and malformed (Fig. 2C,D, and data not shown). In situ hybridization using the *gata6* probe clearly showed impaired liver formation in *hio* mutant embryos at st. 30 (Fig. 2K,L). In addition to the liver defects, *hio* mutant embryos also lacked pectoral fins and died after hatching.

In *kam* mutant embryos, blood accumulated in the liver, and the liver was malformed (Fig. 2E). The expression of *gata6* appeared normal (Fig. 2M).

In *ora* mutant embryos at st. 36, the liver shape was altered, the gall bladder was displaced and the gut undulated (Fig. 2F). *ora* mutant embryos at st. 40 have an enlarged swim bladder and undulated gut, whereas the heart and kidneys appeared unaltered (Fig. 2T,U). Cross sections at the level of the liver, gut tube, and yolk showed that hepatocytes seemed normal, but the embryo itself lay apart from the yolk and the intestine was malformed (Fig. 2P,S). In contrast to regularly aligned polarized epithelial cells in

Table 1
Mutations affecting liver formation and function

Genes	Alleles	Viability	Phenotypes	Other phenotypes	References
Group 1: Mutations affecting liver morphogenesis					
kakurembo (kak)	*j140-3B*	Embryonic lethal	Small and mislocated liver	Mislocated gall bladder, undulated gut	
hiohgi (hio)	*j102-5B*	Embryonic viabe	Small liver	Fin missing	
kamifusen (kam)	*j124-4A*	Embryonic lethal	Malformed liver	Blood accumulated near the liver	
origami (ora)	*j137-1A*	Embryonic viable	Malformed liver	Undulated gut, enlarged swim bladder	
Group 2: Mutations affecting liver laterality					
kendama (ken)	*j103-11C*	Develop to adult fish	Inverted positions of liver and gall bladder	Medially located liver and missing spleen	
hanetsuki (hat)	*j68-7A*	Develop to adult fish	Inverted positions of liver and gall bladder	Inverted heart looping	
dendendaiko (den)	*j73-11A*	Develop to adult fish	Inverted positions of liver and gall bladder	Inverted heart looping	
Group 3: Mutations affecting bile color in the gall bladder					
akane (aka)	*j140-8A*	Embryonic lethal	Deep red bile	Colorless erythrocytes	
suou (suo)	*j98-5A*	Adult viable	Light red bile	Erythrocytes were faint red	
ominaeshi (omi)	*j24-13E*	Embryonic lethal	Colorless bile	Colorless erythrocytes	
Group 4: Mutations affecting lipid metabolism					
ukon (uko)	*j152-8A*	Embryonic lethal	Failure in metabolizing PED6	Edematic after hatching	a
aonibi (aon)	*j60-3A/j9-2F*	Embryonic lethal	Failure in metabolizing PED6	Small and degenerated forebrain at st. 38	
uguisucha (ugu)	*j153-9A*	Embryonic lethal	Failure in metabolizing PED6	Growth retardation after hatching	
Group 5: Mutations affecting endoderm formation					
akatsuki (aku)	*j22-15A/jf121-1A*	Embryonic lethal	Lacking *foxA3* expression	Similar to the zebrafish *oep* phenotype	a,b
akebono (ake)	*j54-7A*	Embryonic lethal	Lacking *foxA3* expression	Similar to the zebrafish *oep* phenotype	a,b
mochizuki (moc)	*j96-11B*	Embryonic lethal	Lacking *foxA3* expression	Similar to the zebrafish *oep* phenotype	a,b
sakura (sak)	*jr10-4A/j153-3A*	Embryonic lethal	Lacking the hepatic bud	Loss of heart and degeneration of eyes	b
hirame (hir)	*j54-20C*	Embryonic lethal	Defect in hypoblast convergence	Flat embryo	a,b
fukuwarai (fku)	*j8-33A/j93-4A*	Embryonic lethal	Lacking the hepatic bud	Cell polarity and alignment affected	a,b

References: a, Kitagawa et al., 2004; b, Furutani-Seiki et al., 2004.

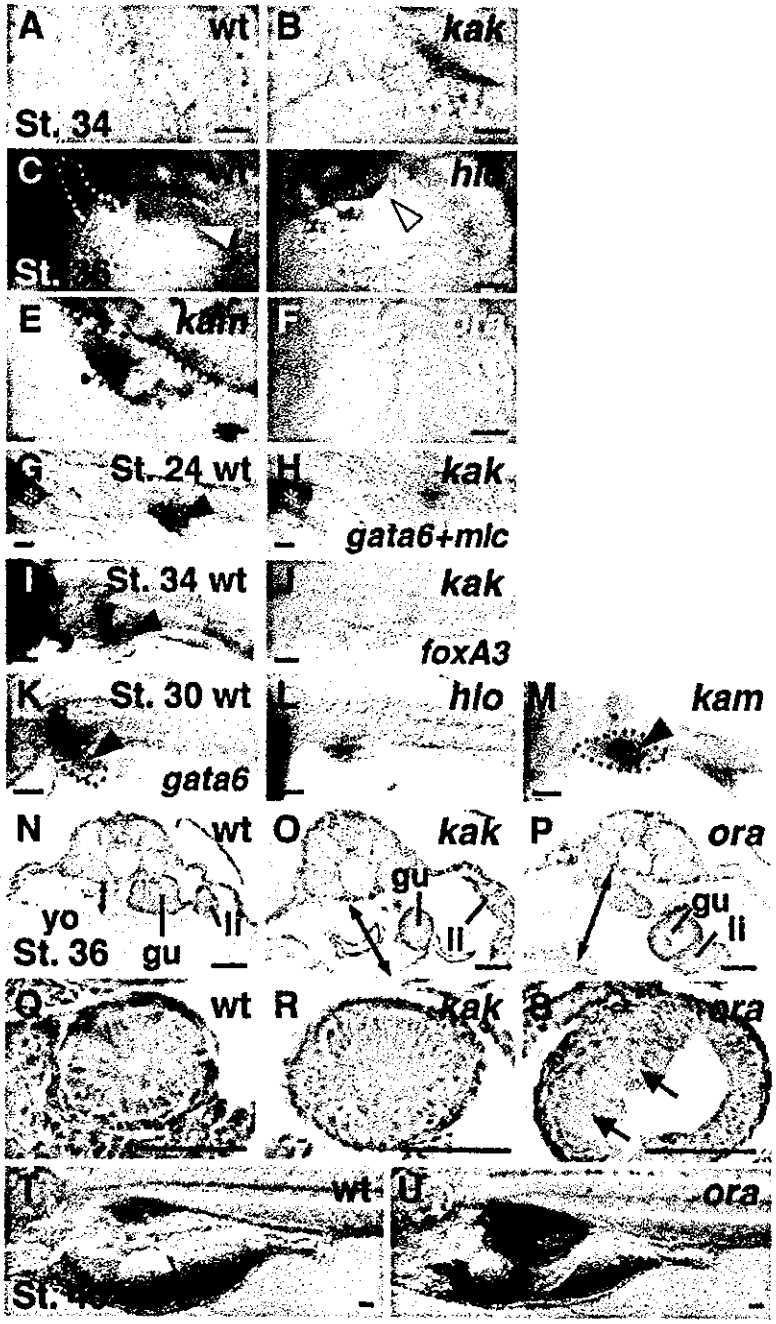

Fig. 2. *kak*, *hio*, *kam* and *ora* mutations affect liver morphogenesis. (A–F, T, and U) Live embryos; (G–M) Fixed embryos stained by in situ hybridization; (N–S) Histological sections stained with hematoxylin and eosin. in situ hybridization was performed using the probes of (G and H) *gata6* and *mlc*; (I and J) *foxA3*; and (K–M) *gata6*. (Q–S) Enlarged view of (N–P), respectively. (A–F, K–M, T and U) Lateral views, (G and H) dorsal views, anterior to the left, (N–S) Cross-sections. (A and B) st. 34; (C–F) st. 36; (G and H) st. 24; (I and J) st. 34; (K–M) st. 30; (N–S) st. 36; (T and U) st. 40. (A, C, G, I, K, N, Q, and T) Wild-type sibling embryos; (B, D, F, H, J, L, M, O, P, R, S, and U) Mutant embryos of (B, H, J, O, and R) *kak*; (D and L) *hio*; (E and M) *kam*; (F, P, S, and U) *ora*. Both arrows indicate the space between the yolk and the embryo proper. White broken lines demarcate the liver. Black and white arrowheads and white asterisks indicate the hepatic bud, gall bladder, and heart, respectively. Black arrows indicate the affected epithelial structure of the gut in the *ora* mutant. Gu: gut, Li: liver, yo: yolk. Scale bars correspond to 50 μm.

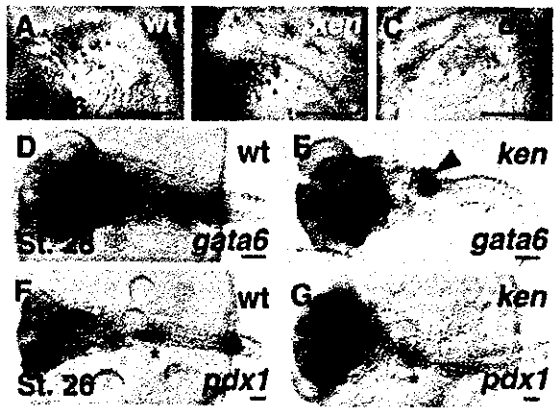

Fig. 3. *ken* and *den* mutations affect liver laterality. (A–C) Live embryos; (D–G) Embryos stained by in situ hybridization using the *gata6* (D and E) and *pdx1* (F and G) probes. (A–C) Lateral views, (D–G) dorsal views, (A, B, D–G) anterior to the left, (C) anterior to the right. (A and D) Wild-type sibling embryos; (B, C, E, and G) Mutant embryos, (B and E) *ken*, (C) *den* mutant embryos. White broken lines demarcate the livers. Black arrowheads, white arrowheads, and black asterisks indicate the liver, gall bladder, and pancreas, respectively. Scale bars correspond to 150 μm.

wild-type embryos, epithelial cells were irregularly arranged in *ora* mutant embryos (arrows in Fig. 2S).

2.2.2. Mutations affecting liver laterality

Mutations in three genes, *kendama* (*ken*), *dendendaiko* (*den*) and *hanetsuki* (*hat*), caused altered liver laterality (Fig. 3). In addition to the liver, the gall bladder, hepatic vein and blood vessels from the liver to the Cuvierian duct were also inverted in these mutant embryos. All mutant embryos hatched and their larvae swam well, suggesting that the altered laterality of the liver and other organs do not affect embryonic viability.

In *ken* mutant embryos, the laterality of the liver and heart was found to be uncoupled, as shown in Table 2. *ken* mutant embryos are classified into four groups according to the location of the liver and heart: (1) the liver shifts to the center and the heart is normally located, L(c)H(n); (2) the liver shifts to the center and the heart was inverted, L(c)H(i); (3) the liver shifts to the right with the heart normally positioned, L(r)H(n); (4) the liver shifts to the right and the heart was inverted, L(r)H(i). These phenotypes were observed in subsequent generations. A *ken* mutant embryo of L(c)H(n) at st. 36 is shown in Fig. 3B. In the embryo in which the liver and gall bladder were located at the center of the body, the liver was not visible from the left view but the heart was observed at the normal location (data not shown). Since, in Medaka the pancreas, detected by the expression of *pdx1*, lies at the center of embryos in the wild-type embryo at st. 26 (Assouline et al., 2001), we could not determine the laterality of the pancreas in *ken* mutant embryos (Fig. 3F,G).

In *den* and *hat* mutant embryos, the liver, gall bladder, and the heart were all inverted in these mutants, as shown in Fig. 3C and Table 2. These results suggest that while *den* and *han* are required for the general laterality of the body, *ken* is required for coupling the laterality of the liver and heart.

2.2.3. Mutations affecting color of bile in the gall bladder

Mutations in three genes, *suou* (*suo*), *akane* (*aka*) and *ominaeshi* (*omi*), affected the color of bile in the gall bladder (Fig. 4). Bile in the wild-type embryo at st. 35 was light green, as shown in Fig. 4A. The bile colors in the three mutants, *suo*, *aka* and *omi*, were orange, deep red and white, respectively (Fig. 4B–D). *aka* and *omi* mutant embryos were embryonic lethal, but *suo* mutant embryos hatched and *suo* homozygotes were fertile.

To determine whether these mutations affect either erythropoiesis or hemoglobin-bile metabolism, we first carried out hemoglobin staining with *o*-dianisidine. As shown in Fig. 4E–H, the blood vessels and heart, but not the gall bladder, were stained in *suo* mutant embryos, but were not stained in *aka* and *omi* mutant embryos. We next examined the expression of *globin* genes by in situ hybridization. Medaka embryos express three types of *globin*, *α-0*, *α-1*, and *β-1* (Maruyama et al., 2002). *α-0*, *α-1*, and *β-1 globins* were expressed in *suo* mutants at st. 33 (Fig. 4I,J,M,N, and data not shown), whereas *α-0*, but not *α-1* and *β-1 globins* were expressed in *aka* mutant embryos (Fig. 4K,O, and data not shown). None of *α-0*, *α-1*, and *β-1 globins* were expressed in *omi* mutant embryos (Fig. 4L,P, and data not shown). These results indicate that *aka* and *omi* mutations affect erythropoiesis. On the other hand,

Table 2
Frequency of alteration of liver and heart laterality

		Laterality phenotype (%)						
		Total	L(l) H(n)	L(l) H(i)	L(c) H(n)	L(c) H(i)	L(r) H(n)	L(r) H(i)
ken	mut	39	0	0	10 (26)	16 (40)	3 (7)	10 (26)
	sib	102	101 (99)	1 (1)	0	0	0	0
hat	mut	21	0	0	0	0	0	21 (100)
	sib	96	95 (99)	1 (1)	0	0	0	0
den	mut	19	0	0	0	0	1 (6)	18 (94)
	sib	120	119 (99)	1 (1)	0	0	0	0

L, liver; H, heart; l, left; c, center; r, right; n, normal; i, invert.

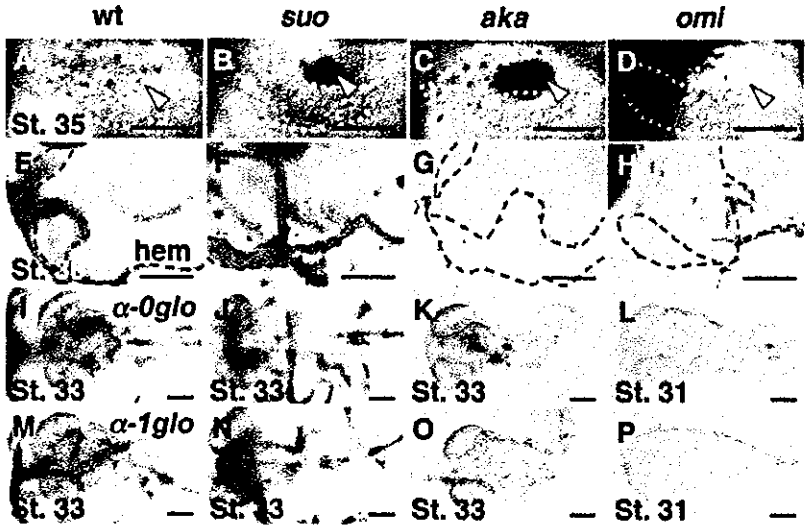

Fig. 4. *aka*, *suo* and *omi* mutations affect bile color. (A–D) Live embryos; (E–H) Hemoglobin staining; (I–P) in situ hybridization, using (I–L) the *α-0 globin*, and (M–P) *α-1 globin* probes. (A–D) st. 35; (E–H) st. 36; (I–K, M–O) st. 33 and (L and P) st. 31. (A, E, I, and M) wild-type sibling embryos, (B, F, J, and N) *suo*, (C, G, K, and O) *aka* and (D, H, L, and P) *omi* mutant embryos. White arrowheads and white broken lines indicate the gall bladder and margin of the liver, respectively. Black broken lines show the Cuvierian duct. Black to brownish spots are melanophores on the yolk. Scale bars correspond to 200 μm.

erythropoiesis appears normal and orange bile in the gall bladder is not due to the accumulation of erythrocytes in *suo* mutant embryos, suggesting that *suo* mutation may affect hemoglobin–bilirubin metabolism.

2.2.4. Mutations affecting lipid metabolism

The fluorescence intensities of PED6 metabolites markedly decreased in three mutant embryos, *ukon* (*uko*), *aonibi* (*aon*) and *uguisucha* (*ugu*), at st. 35 (Fig. 5C–F). To examine whether the decrease in fluorescence intensity is due to the inability of swallowing PED6, we loaded the three mutant embryos with BODIPY-FL-C5, an unquenched form of PED6. All the mutants swallowed the unquenched form of PED6, and the gut, liver and gall bladder showed fluorescence as wild-type embryos (Fig. 5G–J).

uko and *aon* mutant embryos appeared normal in the morphologies of the liver, gall bladder and intestine at st. 35 as shown in Fig. 5B, and *ugu* mutant embryos started to show retardation in development from st. 35 (data not shown). *uko* mutant embryos could hatch but their larvae died a few days after hatching (data not shown). Both *aon* and *ugu* mutant embryos were embryonic lethal. The forebrain was reduced in size from st. 23 in *aon* mutant embryos (Kitagawa et al., 2004). These results suggest that the *uko*, *aon* and *ugu* genes are required for the metabolism or transport of lipids in the hepatobiliary system.

2.2.5. Mutations affecting patterning of endoderm

Six mutations affecting formation of the endodermal rod and/or hepatic bud were identified. Mutations in the *fukuwarai* (*fku*) genes affected endodermal rod morphogenesis (Fig. 6G). Although in *fku* mutant embryos *foxA3* was expressed in the pharynx, hepatic region and the gut (Fig. 6, open circle, arrow head and asterisk, respectively), parts of the endodermal rod were randomly dislocated (Fig. 6G arrow) as other epithelial structures, such as the head structures originated from neuroepithelium (Fig. 6B closed arrow, Kitagawa et al., 2004).

In *sakura* (*sak*) mutant embryos, *foxA3* was expressed in the gut and hepatic region, but not in the pharynx (Fig. 6H). Growth of the hepatic region appeared to be affected and anterior part of the endodermal rod may be missing or misspecified. In *sak* mutant embryos, the heart was not formed and the eyes became degenerated at st. 28 (Fig. 6C, closed arrow).

In embryos with mutations in three genes, *akatsuki* (*aku*), *akebono* (*ake*) and *mochizuki* (*moc*), the endodermal rod was missing (Fig. 6I, data not shown). These mutants exhibited a body patterning phenotypes similar to those of *one-eyed-pinhead* (*oep*) zebrafish mutants (Fig. 6D, data not shown, Kitagawa et al., 2004). While embryos with mutations in only one gene exhibit the *oep* mutant phenotypes, those in three genes display similar phenotypes in both body patterning and endoderm formation.

In *hirame* (*hir*) mutant embryos, *foxA3* expressing endodermal cells did not converge properly, affecting the endermal rod formation (Fig. 6J open arrow). *hir* mutant embryos were flat and tissues such as the lens and heart were mislocated (Fig. 6E, the closed arrow indicates mislocated lens, Kitagawa et al., 2004).

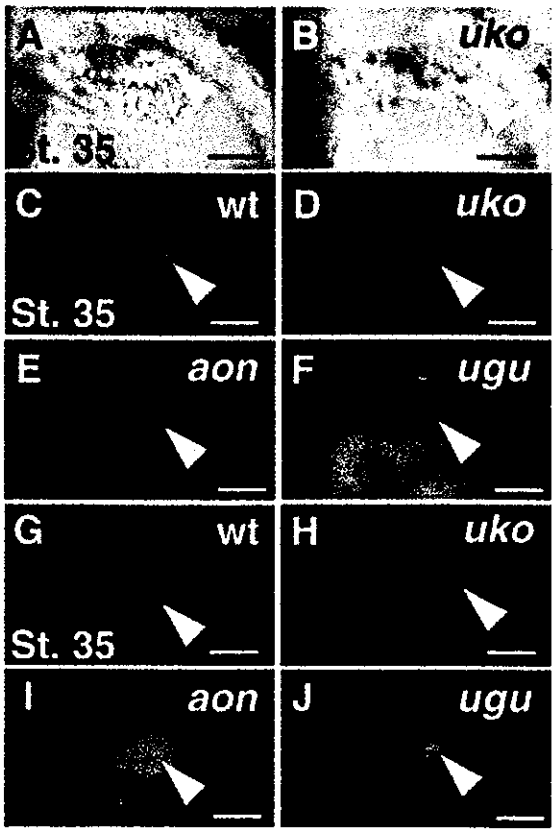

Fig. 5. *uko*, *ugu*, and *aon* mutations affect lipid metabolism. Lateri view, anterior to the left. Live embryos of unstained (A, B), stained with PED6 (C–F) and BODIPY FL-C5 (G–J) at st. 35. (A, C, and G) Wild-type, (B, D, and H) *uko*, (E and I) *aon* and (F and J) *ugu*. Metabolized PED6 (C-F) or BODIPY FL-C5 (G–J) can been seen as a green emission (Em: 505 nm) in the gall bladder (white arrowheads). White broken lines demarcate the margin of the liver. Scale bars correspond to 200 μm.

3. Discussion

3.1. Screening for mutations affecting liver development in Medaka

Partly due to the functional overlap of genes, particularly in vertebrates, mutagenesis screens in a single species are unlikely to be sufficient for identifying all essential genes involved in a particular biological process Therefore, mutagenesis screens and analyses of Medaka mutants complement those in zebrafish, in identifying a wider repertoire of genes by a forward genetic approach in vertebrates.

Our mutagenesis screen in Medaka identified mutations in 19 genes affecting various aspects of the development of the liver and associated tissues. These mutations are classified into five groups: (1) mutations affecting liver morphogenesis; (2) mutations affecting liver laterality; (3) mutations affecting of bile color; (4) mutations affecting lipid metabolism; and (5) mutations affecting endoderm and hepatic bud formation. In zebrafish, a mutagenesis screen using GFP-transgenic fish, whose developing endoderm or organs arising from endoderm are more conspicuous, is underway (D. Y. R. Stainier, personal communication). Thus, mutagenesis screens in both Medaka and zebrafish should be complementary in identifying conserved and divergent mechanisms of liver development.

In our screen, we initially aimed to identify mutations affecting formation and function of the liver specifically. To this end we carried out a screen by multiple criteria to reveal the specificity of the defect. Majority of mutations that we identified were those affecting tissues in addition to the liver during development. From these results, we deduced that mutations affecting the liver specifically may be very limited and that even if defects are not confined to the liver, mutated genes are important for the formation of the liver or physiological functions in which the liver is involved. Thus expression of these genes identified in our screen may not be restricted to the liver but to the tissues, from which the liver originates or those working with the liver to exert its physiological functions.

3.2. Mutations affecting liver morphogenesis

Several explanations may account for the phenotypes of Group 1 mutants with defects in the liver, and gall bladder and gut. First, cell-autonomous defects may affect the regional morphogenesis of the endodermal rod, resulting in altered morphologies of the liver, gall bladder and gut. Second, non-cell-autonomous defects such as the interaction between the surrounding lateral mesoderm and endodermal rod may cause the phenotype. Third, there may be regulatory interactions among the hepatic bud, primordium of the gall bladder and the intestinal bulb. Transplantation experiments to determine the cell autonomy of these mutations would be useful to clarify these possibilities. Finally, since nutrients absorbed from the intestine are metabolized in the liver (Wallace and Pack, 2003; Warga and Stainier, 2002), a defect in the intestine may affect liver growth. The idea that the timing of liver growth is dependent on nourishment from the intestine needs to be further investigated.

In *kak* mutants, although the hepatic bud is formed, the liver is very small at st. 34 and the gall bladder may have shifted its position due to the small liver. This suggests that *kak* is required for the formation of the liver from the hepatic bud.

In *hio* mutants, the liver is small and malformed and the pectoral fin is missing. In zebrafish, some mutations affect the pectoral fin, but no mutations have been reported to affect both the liver and pectoral fin yet (Grandel and Schulte-Merker, 1998; Neumann et al., 1999; van Eeden et al., 1996). It has been suggested that, however, mesodermal components or FGF signaling is

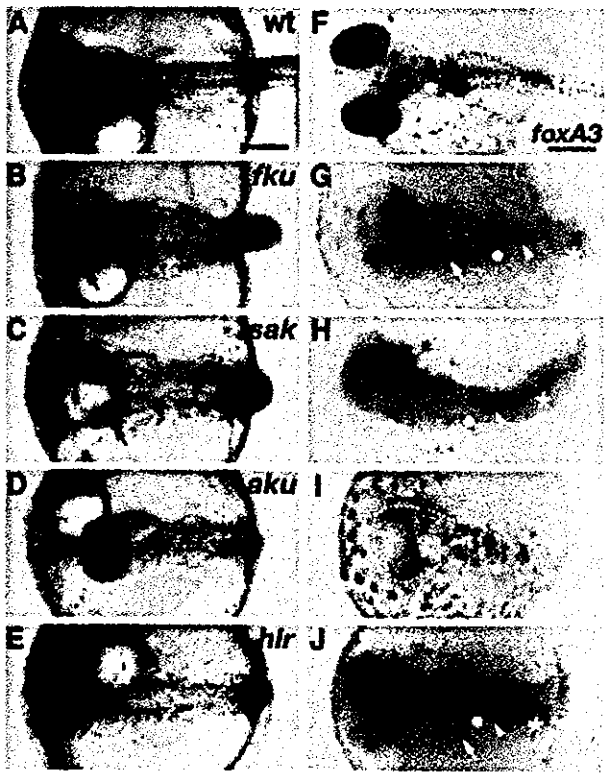

Fig. 6. *fku, sak, aku,* and *hir* mutations affect patterning of endoderm. Dorsal views of (A–E) live embryos and (F–J) embryos stained by in situ hybridization using the *foxA3* probe at st. 28. (A and F) Wild-type embryos, (B and G) *fku*; (C and H) *sak*, (D and I) *aku* and (E and J) *hir* mutant embryos. Open circle, arrowhead, and asterisk indicate the sites where pharynx, hepatic bud, and the gut are normally formed, respectively. Closed arrows show dislocated head structure in B, degenerating eye in C, dislocated lens in E. Open arrows indicate mislocated part of the endodermal rod in G and *foxA3* positive cells inappropriately converged in J. The margin of the embryo was demarcated by the broken line in I. Scale bars correspond to 250 μm.

required for the formation of the pectoral fin and liver (Fischer et al., 2003; Jung et al., 1998; Martin, 1998). It would be interesting to examine mesoderm development and FGF expression in *hio* mutant embryos to further characterize this mutation.

In *kam* mutant embryos, in addition to a malformed liver and gall bladder, the heart is small and blood accumulates near the liver and gut. Such blood accumulation may reflect a defect either in vasculature formation in the liver or in endothelial cell development. In *vegfr2/flk-1* mutant mice with endothelial cell defects, liver budding does not occur. However, in zebrafish, although *cloche* zebrafish mutants lacking all endothelial cells, normal liver budding and development occurs (Field et al., 2003; Stainier et al., 1995). However, severe cardiac edema did not allow analysis of the requirement of endothelial cells during the growth of the liver in those studies. In *kam* mutants, liver budding seems to occur normally, but the growth of the liver may be affected. Detailed analysis of *kam* mutants at the budding and growth periods using endothelial markers would be useful for the further characterization of this mutation.

3.3. Laterality of the liver and other organs

The laterality of all the organs is inverted in most of mutants of zebrafish and mice (Essner et al., 2000; Faucourt et al., 2001; Mochizuki et al., 2002; Schilling et al., 1999), but there are a few reports on uncoupled laterality of the organs (Bisgrove et al., 2000; Field et al., 2003). In zebrafish *flh* and *boz* mutants, the laterality of the liver and heart is randomized and uncoupled (Chin et al., 2000). *flh* is required for specification of the chordamesoderm and *boz* is required for dorsal axis formation. Both *flh* and *boz* are required for early specification of the notochord. Collectively, *ken* mutants show a defect in the laterality of the viscera as observed in *flh* and *boz* mutants but do not show other morphological deficits. An interesting possibility is that *ken* might be a component of the signaling downstream of *boz* and *flh*.

3.4. Mutations affecting bile color

Since a compromised function of the liver readily results in jaundice in human, hemoglobin metabolism producing bilirubin is one of the most important functions of the liver

Hereditary diseases affecting bilirubin metabolism are known in human (Nowicki and Poley, 1998).

Mutations affecting the color of bile in the gall bladder and red blood cells were identified in zebrafish (Ransom et al., 1996; Shafizadeh et al., 2002; Thisse and Zon, 2002; Weistein et al., 1996). *aka* and *omi* mutations also affect erythropoiesis in Medaka. In contrast, *suo* mutation seems to be the first mutation affecting hemoglobin–bilirubin metabolism in zebrafish and Medaka. It would be of interest if *suo* mutation models a human disease.

3.5. Lipid metabolism

PED6 is a substrate for PLA_2 cleavage and a sensitive reporter of its enzymatic activity in vivo (Farber et al., 2001). PLA_2 is important in the generation of lipid signaling molecules, host defenses, lipid absorption and cancer. It is thus a good chemical reagent for screening mutations affecting lipid metabolism. Using PED6, four mutations affecting digestive organ morphology and one mutation affecting bile synthesis or secretion were identified in zebrafish (Farber et al., 2001).

The *uko, aon,* and *ugu* mutations may affect steps in the lipid metabolism pathway, such as ingestion and cleavage of the lipid within the intestine, and subsequent hepatobiliary transport to the gall bladder (Faber et al., 2001). Further biochemical characterization is necessary to determine which component of lipid metabolism is affected in Group 4 mutants.

3.6. Mutations affecting endoderm formation and patterning

The phenotypes of *aku, ake* and *moc* mutants in patterning of the body, endoderm and mesoderm, are similar to those of zebrafish *oep* mutants with defects in the Nodal signaling pathway (Schier et al., 1996, 1997; Zhang et al., 1998). Zebrafish mutations in other components of the Nodal signaling pathway, such as *cyclops, squint* and *smalspur*, exhibit phenotypes substantially different from that of *oep* mutation (Brand et al., 1996). Cloning of three genes, *aku, ake* and *moc* genes will clarify the conserved or divergent functions of these genes in endoderm specification.

The *fku* and *hir* mutants show unique phenotypes in the patterning of the body, not recorded yet in the collection of zebrafish mutants. In *fku* mutants, parts of the head, such as the eyes and nose, are mislocated. In *hir* mutants, the body becomes thinner and several tissues, such as the lens and heart, are mislocated. Although the endodermal cells expressing *foxA3* are present, morphogenesis of the hepatic bud and convergence of the endodermal cells did not occur properly in *fku* and *hir* mutants, respectively. Interestingly, the common feature between *fku* and *hir* mutants is the marked defect of cell alignment in the epithelium (Furutani-Seiki et al., unpublished results). Further analysis of *fku* and *hir* mutants using early hepatocyte markers may help clarify the relationship between endodermal epithelialization and morphogenesis or specification of the endodermal rod.

In *sak* mutants, the heart primordium and the anterior part of the endodermal rod are not formed. It has been reported that the cardiac mesoderm is necessary for the induction of hepatic bud in mice (Duncan, 2003; Jung et al., 1999; Rossi et al., 2001). Further investigation of the requirement of *sak* in the heart or liver by transplantation experiments may provide insights into tissue interactions in heart and liver development.

4. Experimental procedures

4.1. Maintenance of fish stocks

Fish maintenance and mating were carried out as described elsewhere (Furutani-Seiki et al., 2004). Briefly, the Kyoto-Cab sub-strain and Kaga strain were used to induce mutations in the male germline by treatment with ENU (Ethyl-Nitroso-Urea). F3 progenies homozygous for induced mutations were generated by a three generation incrossing scheme.

4.2. Screening procedures

Live F3 progenies were screened for developmental defects at st. 32 and 36 using a Leica MZ12.5 dissecting microscope. For functional screening, we used PED6, a fluorescent PLA_2-substrate dye. PLA_2 cleavage liberates the BODIPY-acyl chain of PED6, resulting in unquenching and green fluorescent emission as described previously (Farber et al., 2001). As the control, BODIPY FL-C5, an unquenched form of PED6 was used. Embryos at st. 35 were placed in 0.5 ml of 1 × Balanced Salt Solution (BSS; 110 mM NaCl, 5 mM KCl, 1 mM $CaCl_2$, and 2.2 mM $MgSO_4$, pH 7.2), containing 0.3 μg/ml PED6 or 0.2 μg/ml BODIPY-FL-C5, and incubated in the dark for 4 h at 28 °C. The embryos were then rinsed with 1 × BSS and placed in a glass depression slide. Using a Zeiss Axioplan 2 microscope, samples were examined for fluorescence from PED6 or BODIPY-FL-C5.

4.3. Histological sections

Embryos were dechorionated and fixed in 4% paraformaldehyde in PBS(−) overnight at 4 °C. The embryos were dehydrated with ethanol and stored at −20 °C. For sectioning, they were incubated in xylene and embedded in paraffin at 67 °C. Paraffin embedded embryos were sectioned (4 μm thickness) and stained with hematoxylin and eosin.

4.4. In situ hybridization

Whole mount in situ hybridization was performed as described elsewhere (Sasado et al., 2004), using an

anti-sense DIG-labeled riboprobe generated from Medaka *foxA3*, *gata6*, *mlc*, *pdx1*, *α-0*, *α-1*, and *β-1 globin* cDNA. Dechorionated embryos were fixed with 4% paraformaldehyde and 0.1% Tween 20 in PBS(−). Embryos later than st. 30 were treated with proteinase K and to remove pigmentation, with H_2O_2. Embryos were photographed using a Leica dissecting microscope.

4.5. Whole embryo staining for hemoglobin expression

Hemoglobin staining was done as described previously (Cocca et al., 1995). Dechorionated embryos were stained for 15 min in the dark in *o*-dianisidine (0.6 mg/ml), 0.01 M sodium acetate (pH 4.5), 0.65% H_2O_2 and 40% (vol/vol) ethanol. Stained embryos were cleared with benzyl benzoate/benzyl alcohol (2:1, vol/vol) and examined with a dissecting microscope.

Acknowledgements

We are grateful to Drs Takashi Sasaki and Noboru Nakajima for cloning *gata6* and *foxA3* probes, Dr Raphael Scharfmann for the *pdx1* probe and to Haruka Momose and Takahiro Negishi for in situ hybridization and graphical works. We would like to thank Drs Shuji Terai and Kiwamu Okita for continual discussion and encouragement. This work was supported by the ERATO project of the Japan Science and Technology Agency to H.K.

References

Alexander, J., Stainier, D.Y., 1999. A molecular pathway leading to endoderm formation in zebrafish. Curr. Biol. 9, 1147–1157.

Assouline, S., Nir, S., Lahav, N., 2001. Simulation of non-enzymatic template-directed synthesis of oligonucleotides and peptides. J. Theor. Biol. 208, 117–125.

Bisgrove, B.W., Essner, J.J., Yost, H.J., 2000. Multiple pathways in the midline regulate concordant brain, heart and gut left-right asymmetry. Development 127, 3567–3579.

Brand, M., Heisenberg, C.P., Warga, R.M., Pelegri, F., Karlstrom, R.O., Beuchle, D., Picker, A., Jiang, Y.J., Furutani-Seiki, M., van Eeden, F.J., Granato, M., Haffter, P., Hammerschmidt, M., Kane, D.A., Kelsh, R.N., Mullins, M.C., Odenthal, J., Nusslein-Volhard, C., 1996. Mutations affecting development of the midline and general body shape during zebrafish embryogenesis. Development 123, 129–142.

Chen, J.N., Haffter, P., Odenthal, J., Vogelsang, E., Brand, M., van Eeden, F.J., Furutani-Seiki, M., Granato, M., Hammerschmidt, M., Heisenberg, C.P., Jiang, Y.J., Kane, D.A., Kelsh, R.N., Mullins, M.C., Nusslein-Volhard, C., 1996. Mutations affecting the cardiovascular system and other internal organs in zebrafish. Development 123, 293–302.

Chin, A.J., Tsang, M., Weinberg, E.S., 2000. Heart and gut chiralities are controlled independently from initial heart position in the developing zebrafish. Dev. Biol. 227, 403–421.

Cocca, E., Ratnayake-Lecamwasam, M., Parker, S.K., Camardella, L., Ciaramella, M., di Prisco, G., Detrich, H.W., 1995. Genomic remnants of alpha-globin genes in the hemoglobinless antarctic icefishes. Proc. Natl Acad. Sci. USA 92, 1817–1821.

Douarin, N.M., 1975. An experimental analysis of liver development. Med. Biol. 53, 427–455.

Duncan, S.A., 2003. Mechanisms controlling early development of the liver. Mech. Dev. 120, 19–33.

Essner, J.J., Branford, W.W., Zhang, J., Yost, H.J., 2000. Mesendoderm and left-right brain, heart and gut development are differentially regulated by pitx2 isoforms. Development 127, 1081–1093.

Farber, S.A., Pack, M., Ho, S.Y., Johnson, I.D., Wagner, D.S., Dosch, R., Mullins, M.C., Hendrickson, H.S., Hendrickson, E.K., Halpern, M.E., 2001. Genetic analysis of digestive physiology using fluorescent phospholipid reporters. Science 292, 1385–1388.

Faucourt, M., Houliston, E., Besnardeau, L., Kimelman, D., Lepage, T., 2001. The pitx2 homeobox protein is required early for endoderm formation and nodal signaling. Dev. Biol. 229, 287–306.

Field, H.A., Ober, E.A., Roeser, T., Stainier, D.Y., 2003. Formation of the digestive system in zebrafish. I. Liver morphogenesis. Dev. Biol. 253, 279–290.

Fischer, S., Draper, B.W., Neumann, C.J., 2003. The zebrafish fgf24 mutant identifies an additional level of Fgf signaling involved in vertebrate forelimb initiation. Development 130, 3515–3524.

Furutani-Seiki, M., Sasado, T., Morinaga, C., Suwa, H., Niwa, K., Yoda, H., et al., 2004. A systematic genome-wide screen for mutations affecting organogenesis in Medaka, *Oryzias latipes*. Mech. Dev. 121, 647–658.

Grandel, H., Schulte-Merker, S., 1998. The development of the paired fins in the zebrafish (Danio rerio). Mech. Dev. 79, 99–120.

Grapin-Botton, A., Melton, D.A., 2000. Endoderm development: from patterning to organogenesis. Trends Genet. 16, 124–130.

Jung, J., Zheng, M., Goldfarb, M., Zaret, K.S., 1999. Initiation of mammalian liver development from endoderm by fibroblast growth factors. Science 284, 1998–2003.

Kitagawa, D., Watanabe, T., Saito, K., Asaka, S., Sasado, T., Morinaga, C., et al., 2004. Genetic dissection of the formation of the forebrain in Medaka, *Oryzias latipes*. Mech. Dev. 121, 673–685.

Martin, G.R., 1998. The roles of FGFs in the early developments of vertebrate limbs. Genes Dev. 12, 1571–1586.

Maruyama, K., Yasumasu, S., Iuchi, I., 2002. Characterization and expression of embryonic and adult globins of the teleost *Oryzias latipes* (medaka). J. Biochem. 132, 581–589.

Matsumoto, K., Toshitomi, H., Rossant, J., Zaret, K.S., 2001. Liver organogenesis promoted by endothelial cells prior to vascular function. Science 294, 559–563.

Mochizuki, T., Tsuchiya, K., Yokoyama, T., 2002. Molecular cloning of a gene for inversion of embryo turning (inv) with cystic kidney. Nephrol. Dial. Transplant 17(Suppl. 9), 68–70.

Neumann, C.J., Grandel, H., Gaffield, W., Schulte-Merker, S., Nusslein-Volhard, C., 1999. Transient establishment of anteroposterior polarity in the zebrafish pectoral fin bud in the absence of sonic hedgehog activity. Development 126, 4817–4826.

Nishina, H., Vaz, C., Billia, P., Nghiem, M., Sasaki, T., De la Pompa, J.L., Furlonger, K., Paige, C., Hui, C., Fischer, K.D., Kishimoto, H., Iwatsubo, T., Katada, T., Woodgett, J.R., Penninger, J.M., 1999. Defective liver formation and liver cell apoptosis in mice lacking the stress signaling kinase SEK1/MKK4. Development 126, 505–516.

Nowicki, M.J., Poley, J.R., 1998. The hereditary hyperbilirubinaemias. Baillieres Clin. Gastroenterol. 12, 355–367.

Ober, E.A., Field, H.A., Stainier, D.Y., 2003. From endoderm formation to liver and pancreas development in zebrafish. Mech. Dev. 120, 5–18.

Pack, M., Solnica-Krezel, L., Malicki, J., Neuhauss, S.C., Schier, A.F., Stemple, D.L., Driever, W., Fishman, M.C., 1996. Mutations affecting development of zebrafish digestive organs. Development 123, 321–328.

Ransom, D.G., Haffter, P., Odenthal, J., Brownlie, A., Vogelsang, E., Kelsh, R.N., Brand, M., van Eeden, F.J., Furutani-Seiki, M., Granato, M., Hammerschmidt, M., Heisenberg, C.P., Jiang, Y.J., Kane, D.A., Mullins, M.C., Nusslein-Volhard, C., 1996. Characterization of zebrafish mutants with defects in embryonic hematopoiesis. Development 123, 311–319.

Rossi, J.M., Dunn, N.R., Hogan, B.L., Zaret, K.S., 2001. Distinct mesodermal signals, including BMPs from the septum transversum

mesenchyme, are required in combination for hepatogenesis from the endoderm. Genes Dev. 15, 1998–2009.

Sasado, T., Morinaga, C., Niwa, K., Shinomiya, A., Yasuoka, A., Suwa, H., et al., 2004. Mutations affecting early distribution of primordial germ cells in Medaka (*Oryzias latipes*) embryo. Mech. Dev. 121, 817–828.

Schier, A.F., Neuhauss, S.C., Harvey, M., Malicki, J., Solnica-Krezel, L., Stainier, D.Y., Zwartkruis, F., Abdelilah, S., Stemple, D.L., Rangini, Z., Yang, H., Driever, W., 1996. Mutations affecting the development of the embryonic zebrafish brain. Development 123, 165–178.

Schier, A.F., Neuhauss, S.C., Helde, K.A., Talbot, W.S., Driever, W., 1997. The one-eyed pinhead gene functions in mesoderm and endoderm formation in zebrafish and interacts with no tail. Development 124, 327–342.

Schilling, T.F., Concordet, J.P., Ingham, P.W., 1999. Regulation of left-right asymmetries in the zebrafish by Shh and BMP4. Dev. Biol. 210, 277–287.

Shafizadeh, E., Paw, B.H., Foott, H., Liao, E.C., Barut, B.A., Cope, J.J., Zon, L.I., Lin, S., 2002. Characterization of zebrafish merlot/chablis as non-mammalian vertebrate models for severe congenital anemia due to protein 4.1 deficiency. Development 129, 4359–4370.

Stainier, D.Y., Weinstein, B.M., Detrich, H.W. 3rd, Zon, L.I., Fishman, M.C., 1995. Cloche, an early acting zebrafish gene, is required by both the endothelial and hematopoietic lineages. Development 121, 3141–3150.

Tam, P.P., Kanai-Azuma, M., Kanai, Y., 2003. Early endoderm development in vertebrates: lineage differentiation and morphogenetic function. Curr. Opin. Genet. Dev. 13, 393–400.

Thisse, C., Zon, L., 2002. Organogenesis-heart and blood formation from the zebrafish point of view. Science 295, 457–462.

van Eeden, F.J., Granato, M., Schach, U., Brand, M., Furutani-Seiki, M., Haffter, P., Hammerschmidt, M., Heisenberg, C.P., Jiang, Y.J., Kane, D.A., Kelsh, R.N., Mullins, M.C., Odenthal, J., Warga, R.M., Nusslein-Volhard, C., 1996. Genetic analysis of fin formation in the zebrafish. Danio rerio. Development 123, 255–262.

Wada, T., Joza, N., Cheng, H.M., sasaki, T., Kozieradzki, I., Bachmaier, K., Katada, T., Schreiber, M., Wagner, E.F., Nishina, H., Penninger, J.M., 2004. MKK7 couples stress signaling to G2/M cell cycle progression and cellular senescence. Nat. Cell Biol. 6, 215–226.

Wallace, K.N., Pack, M., 2003. Unique and conserved aspects of gut development in zebrafish. Dev. Biol. 255, 12–29.

Warga, R.M., Stainier, D.Y., 2002. The guts of endoderm formation. Results Probl. Cell Differ. 40, 28–47.

Watanabe, T., Nakagawa, K., Ohata, S., Kitagawa, D., Nishitai, G., Seo, J., Tanemura, S., Shimizu, N., Kishimoto, H., Wada, T., Aoki, J., Arai, H., Iwatsubo, T., Mochita, M., Satake, M., Ito, Y., Matsuyama, T., Mak, T.W., Penninger, J.M., Nishina, H., Katada, T., 2002. SEK1/MKK4-mediated SAPK/JNK signaling participates in embryonic hepatoblast proliferation via a pathway different from NF-κB-induced anti-apoptosis. Dev. Biol. 250, 332–347.

Weistein, B., Schier, A., Abdelilar, S., Malicki, J., Solnica-Krezel, L., Stemple, D., Stainier, D.Y., Zwartkruis, F., Driever, W., Fishman, M., 1996. Hematopoietic mutations in the zebrafish. Development 123, 303–309.

Zaret, K.S., 2001. Hepatocyte differentiation: from the endoderm and beyond. Curr. Opin. Genet. Dev. 11, 568–574.

Zaret, K.S., 2002. Regulatory phases of early liver development: paradigms of organogenesis. Nat. Rev. Genet. 3, 499–512.

Zhang, J., Talbot, W.S., Schier, A.F., 1998. Positional cloning identifies zebrafish one-eyed pinhead as a permissive EGF-related ligand required during gastrulation. Cell 92, 241–251.

Glossary

hiohgi:	a traditional Japanese hand fan for court functions;
kakurembo:	a game of hide-and-seek;
kamifusen:	a balloon made of paper;
origami:	art of folding paper;
kendama:	Japanese toy with a wooden cup and a ball on a thread, where one tries to catch the ball in the cup;
hanetsuki:	traditional Japanese badminton using colored wooden racquets and a shuttlecock;
dendendaiko:	a Japanse drum for children that makes a sound by turning it upside down;
akane, suou:	traditional Japanese term for red;
ominaeshi:	a traditional Japanese term for white;
uguisucha, ukon:	traditional Japanese dark yellow color;
aonibi:	dark green;
fukuwarai:	Japanese jigsaw-puzzle to make with face blindfolded;
sakura:	cherry blossom;
akebono:	rising sun;
akatsuki, mochizuki:	full moon;
hirame:	flounder

JB Minireview

J. Biochem. **136**, 00–00 (2004)
DOI: 10.1093/jb/mvh117.

Physiological Roles of SAPK/JNK Signaling Pathway

Hiroshi Nishina*, Teiji Wada and Toshiaki Katada

Department of Physiological Chemistry, Graduate School of Pharmaceutical Sciences, University of Tokyo, Tokyo 113-0033

Received May 6, 2004; accepted May 6, 2004

Stress-activated protein kinase/c-Jun NH_2-terminal kinase (SAPK/JNK) is activated by many types of cellular stresses and extracellular signals. Recent studies, including the analysis with knockout mice, have led to progress towards understanding the physiological roles of SAPK/JNK activation in embryonic development in addition to immune responses. SAPK/JNK activation plays essential roles in organogenesis during mouse development by regulating cell survival, apoptosis, and proliferation. Two SAPK/JNK activators, SEK1 and MKK7, are required for fetal liver formation and full activation of SAPK/JNK, which responds to various stimuli in an all-or-none manner. This article focuses on physiological roles of SAPK/JNK activation in fetal liver formation and in apoptosis regulation.

Key words: apoptosis, liver formation, MAP kinase, SAPK/JNK, stress.

Developmental programs and environmental agents trigger distinct and evolutionarily conserved kinases that relay signals mediating survival, death, proliferation, and cell cycle arrest. Mitogen-activated protein kinases (MAPKs) are evolutionarily conserved serine/threonine kinases involved in regulation of many cellular events. Several MAPK groups have been identified in mammalian cells, including extracellular signal-regulated kinase (ERK), p38, and SAPK/JNK. These MAPKs are activated by their specific MAPK kinases (MAPKKs): ERK by MEK1 and MEK2, p38 by MKK3 and MKK6, and SAPK/JNK by SEK1 (also known as MKK4) and MKK7 (SEK2). These MAPKKs are also activated by various MAPKK kinases (MAPKKKs) such as Raf, MLK, MEKK1, TAK1, and ASK1.

SAPK/JNK is ubiquitously expressed and is activated by many types of stress, including UV and γ-irradiation, protein synthesis inhibitors (anisomycin), hyperosmolarity, toxins, ischemia/reperfusion injury in heart attacks, heat shock, anticancer drugs (cisplatinum, adriamycin, or etoposide), ceramide, T-cell receptor stimulation, peroxide, and inflammatory cytokines such as TNFα. Recently, several *in vitro* and *in vivo* experiments have shown that SAPK/JNK is activated synergistically by SEK1 and MKK7. The SAPK/JNK stress pathway participitates in many different intracellular signaling pathways that control a spectrum of cellular processes, including cell proliferation, differentiation, transformation, apoptosis, migration, and cytoskeletal integrity. SAPK/JNK has been reported to phosphorylate transcription factors in addition to c-Jun, such as ATF-2, Elk-1, p53, and c-Myc, as well as nontranscription factors such as Bcl-2, Bcl-xL, paxillin, and MAP2 (*1–6*). This review summarizes recent progress in the SAPK/JNK signaling pathway in mouse development and the molecular mechanism of SAPK/JNK activation.

*To whom correspondence should be addressed. Tel: +81-3-5841-4754, Fax: +81-3-5841-4751, E-mail: nishina@mol.f.u-tokyo.ac.jp

Role of SAPK/JNK in mouse development

All three *Jnk* (*Jnk1*, *2*, and *3*), and *sek1* and *mkk7* loci have been knocked out. JNK1 and JNK2 are widely expressed in many tissues, but JNK3 is expressed predominantly in nervous system. Mice deficient in the single gene of *Jnk1*, *Jnk2*, or *Jnk3*, and *Jnk1/Jnk3*– or *Jnk2/Jnk3*–double mutant mice all survived normally. Mice lacking both JNK1 and JNK2 die around embryonic day 11 (E11) with severe dysregulation of apoptosis in the brain (*7*, *8*). Specifically, there was a reduction of cell death in the lateral edges of the hindbrain prior to neural tube closure. In contrast, increased apoptosis and caspase activation were found in the mutant forebrain. These results assign both pro-and anti-apoptotic functions to JNK1 and JNK2 in the development of the fetal brain.

Sek1$^{-/-}$ embryos die between E10.5 and E12.5 with impaired liver formation and massive apoptosis (*9–12*). We have recently shown that SEK1-mediated SAPK/JNK pathway downstream TNF-α receptor 1 (TNFR1) participates in embryonic hepatoblast proliferation and survival via a pathway different from NF-κB–induced antiapoptosis (*13*). Furthermore, *mkk7*$^{-/-}$ embryos die between E11.5 and E12.5 with similar defects in liver formation (*14*). These results indicate that SEK1 and MKK7 cannot substitute for one another *in vivo* and that both are important for hepatoblast proliferation and survival during mouse embryogenesis (Fig. 1).

Role of SAPK/JNK in apoptosis regulation

It has been proposed that SAPK/JNK activation triggers the mitochondria-dependent apoptosis in response to many types of stress, including UV-irradiation. Both *Jnk1*$^{-/-}$ *Jnk2*$^{-/-}$ and *sek1*$^{-/-}$ *mkk7*$^{-/-}$ mouse embryonic fibroblasts (MEFs) exhibited profound defects in stress-induced apoptosis (*15*, *16*). These results strongly suggest that the SAPK/JNK activation directly regulates mitochondria-dependent apoptosis in the pro-apoptotic direction. In contrast, *sek1*$^{-/-}$ *mkk7*$^{-/-}$ ES cells show normal apoptotic responses, including DNA fragmentation and

© 2004 The Japanese Biochemical Society.

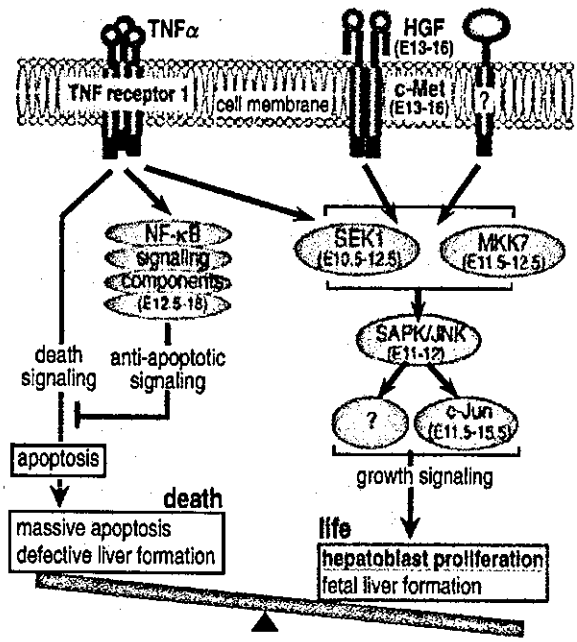

Fig. 1. A proposed model for SAPK/JNK signaling pathway in hepatoblasts. The numbers in parentheses are dates of embryonic lethality reported in previous papers. TNFα elicits a wide range of biological responses, such as inflammation, tumor necrosis, differentiation, cell proliferation, and apoptosis, through the stimulation of its receptor, TNFR1. The induction of apoptosis, NF-κB activation, and SAPK/JNK activation are simultaneously mediated through TNFR1. SAPK/JNK activation is involved in cell proliferation, while activation of NF-κB protects against the apoptosis in hepatoblasts (*13*).

caspase 3 activation, even though *apaf1*$^{-/-}$ ES cells exhibit profound defects in the mitochondria-dependent apoptosis (*17*). In those *sek1*$^{-/-}$ *mkk7*$^{-/-}$ ES cells, the SAPK/JNK activation by various stresses was completely abolished. Normal apoptotic responses without SAPK/JNK activation were also observed in fibroblasts derived from *sek1*$^{-/-}$ *mkk7*$^{-/-}$ ES cells. These results raised the question of whether SAPK/JNK activation is indeed required for the induction of cell death in response to apoptosis inducers. Thus, the physiological role of SAPK/JNK activation in cell survival and apoptosis is controversial, being suggested to have a pro-apoptotic, an anti-apoptotic, or no function (*18*).

From our recent results, it appears that the various roles of SAPK/JNK activation in apoptosis depend on the cell types and conditions observed. While late passage *mkk7*$^{-/-}$ MEFs are resistant to cell death in the same manner as *Jnk1*$^{-/-}$ *Jnk2*$^{-/-}$ and *sek1*$^{-/-}$ *mkk7*$^{-/-}$ MEFs (*15*, *16*), *mkk7*$^{-/-}$ MEFs at earlier cell passages (passages 1–4) undergo apoptosis in response to UV exposure with the same kinetics and to the same extent as wild-type MEFs (*14*). These results support the notion that SAPK/JNK activation is not always involved in apoptosis, but this activation rather regulates apoptosis in a signal-specific (and perhaps cell type-dependent) manner. Our results in MEFs indicate that the 'history' and passage number of cells is a critical determinant of cell death susceptibility in the absence of MKK7 expression.

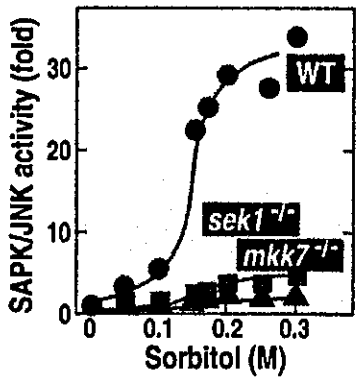

Fig. 2. SAPK/JNK activation in response to hyper-osmolar stress (sorbitol) requires both SEK1 and MKK7 in ES cells. Wild-type, *sek1*$^{-/-}$, and *mkk7*$^{-/-}$ ES cells were stimulated with the indicated concentrations of sorbitol for 30 min.

SAPK/JNK activation as a molecular switch in an all-or-none manner

Recently, Ferrell *et al.* have proposed the interesting concept that SAPK/JNK-signaling cascade could, in principle, function as a sensitivity amplifier, which converts graded inputs into more switch-like outputs, allowing the cascade to filter out noise and yet still respond decisively to supra-threshold stimuli (*19*, *20*). They have shown in *Xenopus* oocytes, HeLa cells, HEK293 cells, and Jurkat T cells that SAPK/JNK responds to physiological and pathological stimuli, such as progesterone and sorbitol, in an all-or-none manner. The activation of SAPK/JNK by the stimuli was graded at the level of a population of oocytes; however, at the level of an individual oocyte, the stimulatory response appeared to be switch-like. Indeed, we have also observed a very steep concentration-dependent response in the activation of SAPK/JNK by hyper-osmolar stress, sorbitol, in wild-type murine embryonic stem (ES) cells but not in *sek1*$^{-/-}$ and *mkk7*$^{-/-}$ cells (Fig. 2) (*21*). This suggests that the all-or-none type MAPK activation also occurs in mammalian cells at an individual cell level only when the two MAPKKs are simultaneously activated. Therefore, this MAPK signaling should strictly proceed without errors basically through two separate signals, one that activates SEK1 and one that activates MKK7. The full activation of SAPK/JNK by SEK1 and MKK7 may be required for hepatoblast proliferation (Fig. 1).

Molecular mechanism of SAPK/JNK activation in living cells

Activation of SAPK/JNK requires the dual phosphorylation of Tyr and Thr residues located in a Thr-Pro-Tyr motif in the activation loop between VII and VIII of the kinase domain. The phosphorylation is catalyzed by the dual specificity kinases, SEK1 and MKK7, which are capable of catalyzing the phosphorylation of both Thr and Tyr residues. Recent studies have shown that SEK1 preferentially phosphorylates the Tyr residue, and MKK7 the

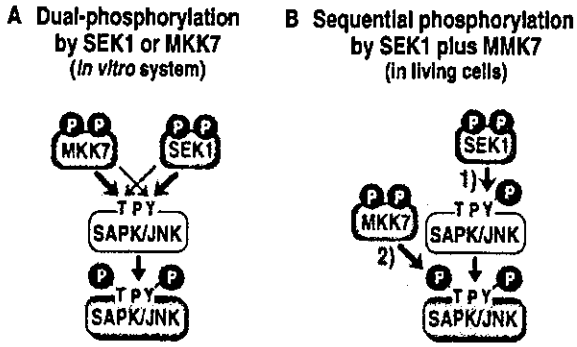

Fig. 3. **Schematic description of SAPK/JNK phosphorylation by SEK1 and MKK7 *in vitro* and *in vivo*.** A: Synergistic activation of SAPK/JNK by the dual-specificity kinase, SEK1 or MKK7, which has been reported in *in vitro* conditions (*22–24*). B: Synergistic activation of SAPK/JNK through sequential phosphorylation by SEK1 and MKK7 in murine living cells (*21, 25*). TPY, Thr-Pro-Tyr motif.

Thr residue of SAPK/JNK *in vitro* (Fig. 3A) (*22–24*). Strong support for this activation mechanism has been obtained from studies of SEK1- and MKK7-gene disruption in ES cells (*21, 25*). The severe impairment of SAPK/JNK activation observed in *mkk7*$^{-/-}$ ES cells was accompanied by a loss of the Thr-phosphorylation of SAPK/JNK, without marked reduction in its Tyr-phosphorylation level. On the other hand, Thr-phosphorylation of SAPK/JNK in *sek1*$^{-/-}$ ES cells was also attenuated, in addition to a decreased level of its Tyr-phosphorylation. These results indicate that the Tyr and Thr residues of SAPK/JNK are sequentially phosphorylated by SEK1 and MKK7, respectively, in stress-stimulated living cells (Fig. 3B).

Conclusion

SAPK/JNK activation by SEK1 and MKK7 is required for embryonic hepatoblast proliferation. The full activation of SAPK/JNK occurs only when the two MAPKKs are simultaneously activated. The Tyr and Thr residues of SAPK/JNK are sequentially phosphorylated by SEK1 and MKK7, respectively, in living cells.

SAPK/JNK may either protect or enhance sensitivity to apoptosis depending on the cell type, stimuli, and the latency of the activation of the MAPK. Our recent results in MEFs indicate that the "history" and passage number of cells are a critical determinant of cell death susceptibility in the absence of MKK7 expression. In this apoptotic pathway, SAPK/JNK seems to function through its effects on gene expression but not a direct effect on the effectors of apoptosis. These new findings could also solve the controversial data that have been obtained in different cell types and in different laboratories.

REFERENCES

1. Davis, R.J. (2000) Signal transduction by the JNK group of MAP kinases. *Cell* **103**, 239–252
2. Chang, L. and Karin, M. (2001) Mammalian MAP kinase signalling cascades. *Nature* **410**, 37–40
3. Weston, C.R. and Davis, R.J. (2002) The JNK signal transduction pathway. *Curr. Opini. Genes Dev.* **12**, 14–21
4. Manning, A.M. and Davis, R.J. (2003) Targeting JNK for therapeutic benefit: from junk to gold? *Nat. Rev. Mol. Drug Disc.* **2**, 554–565
5. Nishina, H., Nakagawa, K., Azuma, N., and Katada, T. (2003) Activation mechanism and physiological roles of stress-activated protein kinase/c-Jun NH_2-terminal kinase in mammalian cells. *J. Biol. Regul. Homeost. Agents.* **17**, 295–302
6. Wada, T. and Penninger, J.M. (2004) Mitogen-activated protein kinases in apoptosis regulation. *Oncogene* **23**, 2838–2849
7. Kuan, C.Y., Yang, D.D., Roy, D.R., Davis, R.J., Rakic, P., and Flavell, R.A. (1999) The Jnk1 and Jnk2 protein kinases are required for regional specific apoptosis during early brain development. *Neuron* **22**, 667–676
8. Sabapathy, K., Jochum, W., Hochedlinger, K., Chang, L., Karin, M., and Wagner, E.F. (1999) Defective neural tube morphogenesis and altered apoptosis in the absence of both JNK1 and JNK2. *Mech. Dev.* **89**, 115–124
9. Nishina, H., Fischer, K.D., Radvanyi, L., Shahinian, A., Hakem, R., Rubie, E.A., Bernstein, A., Mak, T.W., Woodgett, J.R., and Penninger, J.M. (1997) Stress-signalling kinase Sek1 protects thymocytes from apoptosis mediated by CD95 and CD3. *Nature* **385**, 350–353
10. Yang, D., Tournier, C., Wysk, M., Lu, H.T., Xu, J., Davis, R.J., and Flavell, R.A. (1997) Targeted disruption of the MKK4 gene causes embryonic death, inhibition of c-Jun NH2-terminal kinase activation, and defects in AP-1 transcriptional activity. *Proc. Natl Acad. Sci. USA* **94**, 3004–3009
11. Ganiatsas, S., Kwee, L., Fujiwara, Y., Perkins, A., Ikeda, T., Labow, M.A., and Zon, L.I. (1998) SEK1 deficiency reveals mitogen-activated protein kinase cascade crossregulation and leads to abnormal hepatogenesis. *Proc. Natl Acad. Sci. USA* **95**, 6881–6886.
12. Nishina, H., Vaz, C., Billia, P., Nghiem, M., Sasaki, T., Pompa, J.L., Furlonger, K., Paige, C., Hui, C.-C., Fischer, K.D., Kishimoto, H., Iwatsubo, T., Katada, T., Woodgett, J.R., and Penninger, J.M. (1999) Defective liver formation and liver cell apoptosis in mice lacking the stress signaling kinase SEK1/MKK4. *Development* **126**, 505–516
13. Watanabe, T. Nakagawa, K, Ohata, S, Kitagawa, D., Nishitai, G., Seo, J., Tanemura, S., Shimizu, N., Kishimoto, H., Wada, T., Aoki, J., Arai, H., Iwatsubo, T., Mochita, M., Watanabe, T., Satake, M., Ito, Y., Matsuyama, T., Mak, T.W., Penninger, J.M., Nishina, H., and Katada, T. (2002) SEK1/MKK4-mediated SAPK/JNK signaling participates in embryonic hepatoblast proliferation via a pathway different from NF-κB-induced antiapoptosis. *Dev. Biol.* **250**, 332–347
14. Wada, T., Joza, N., Cheng, H.-Y.M., Sasaki, T., Kozieradzki, I., Bachmaier, K., Katada, T., Schreiber, M., Wagner, E.F., Nishina, H., and Penninger, J.M. (2004) MKK7 couples stress signaling to G2/M cell cycle progression and cellular senescence. *Nat. Cell Biol.* **6**, 215–226
15. Tournier, C., Hess, P., Yang, D.D., Xu, J., Turner, T.K., Nimnual, A., Bar-Sagi, D., Jones, S.N., Flavell, R.A., and Davis, R.J. (2000) Requirement of JNK for stress-induced activation of the cytochrome c-mediated death pathway. *Science* **288**, 870–874
16. Tournier, C., Dong, C., Turner, T.K., Jones, S.N., Flavell, R.A., and Davis, R.J. (2001) MKK7 is an essential component of the JNK signal transduction pathway activated by proinflammatory cytokines. *Genes Dev.* **15**, 1419–1426
17. Nishitai, G., Shimizu, N., Negishi, T., Kishimoto, H., Nakagawa, K., Kitagawa, D., Watanabe, T., Momose, H., Ohata, S., Tanemura, S., Asaka, S., Kubota, J., Saito, R., Yoshida, H., Mak, T.W., Wada, T., Penninger, J.M., Azuma, N., Nishina, H., and Katada, T. (2003) Stress induces mitochondria-mediated apoptosis independent of SAPK/JNK activation in ES cells. *J. Biol. Chem.* **279**, 1621–1626
18. Lin, A. (2002) Activation of the JNK signaling pathway: breaking the brake on apoptosis. *Bioessays* **25**, 17–24

19. Bagowski, C.P. and Ferrell, J.E. (2001) Bistability in the JNK cascade. *Curr. Biol.* **11**, 1176–1182
20. Bagowski, C.P., Besser, J., Frey, C.R., Ferrell, J.E. (2003) The JNK cascade as a biochemical switch in mammalian cells: Ultrasensitive and all-or-none responses. *Curr. Biol.* **13**, 315–320
21. Kishimoto, H., Nakagawa, K., Watanabe, T., Kitagawa, D., Momose, H., Seo, J., Nishitai, G., Shimizu, N., Ohata, S., Tanemura, S., Asaka, S., Goto, T., Fukushi, H., Yoshida, H., Suzuki, A., Sasaki, T., Wada, T., Penninger, J.M., Nishina, H., and Katada, T. (2003) Different Properties of SEK1 and MKK7 in Dual Phosphorylation of Stress-induced Activated Protein Kinase SAPK/JNK in Embryonic *Stem Cells. J. Biol. Chem.* **278**, 16595–16601
22. Lawler, S., Fleming, Y., Goedert, M., and Cohen, P. (1998) Synergistic activation of SAPK1/JNK1 by two MAP kinase kinases *in vitro*. *Curr. Biol.* **8**, 1387–1390
23. Lisnock, J., Griffin, P., Calaycay, J., Franz, B., Parsons, J., O'Keefe, S.J., and LoGrasso, P. (2000) Activation of JNK3α1 requires both MKK4 and MKK7: Kinetic characterization of *in vitro* phosphorylated JNK3α1. *Biochemistry* **39**, 3141–3148
24. Fleming, Y., Armstrong, C.G., Morrice, N., Paterson, A., Goedert, M., and Cohen, P. (2000) Synergistic activation of stress-activated protein kinase 1/c-Jun N-terminal kinase (SAPK1/JNK) isoforms by mitogen-activated protein kinase 4 (MKK4) and MKK7. *Biochem. J.* **352**, 145–154
25. Wada, T., Nakagawa, K., Watanabe, T., Nishitai, G., Seo, J., Kishimoto, H., Kitagawa, D., Sasaki, T., Penninger, J.M., Nishina, H., and Katada, T. (2001). Impaired synergistic activation of stress activated protein kinase SAPK/JNK in mouse embryonic stem cells lacking SEK1/MKK4. *J. Biol. Chem.* **276**, 30892–30897

Journal of Neuroscience Research 76:265–276 (2004)

Blockade of Interleukin-6 Receptor Suppresses Reactive Astrogliosis and Ameliorates Functional Recovery in Experimental Spinal Cord Injury

S. Okada,[1–3] M. Nakamura,[4] Y. Mikami,[4] T. Shimazaki,[1,3] M. Mihara,[5] Y. Ohsugi,[5] Y. Iwamoto,[2] K. Yoshizaki,[6] T. Kishimoto,[7] Y. Toyama,[4] and H. Okano[1,3]*

[1]Department of Physiology, Keio University School of Medicine, Shinjuku, Tokyo, Japan
[2]Department of Orthopedic Surgery, Graduate School of Medical Sciences, Kyushu University, Fukuoka, Japan
[3]Core Research for Evolutional Science and Technology (CREST), Japan Science and Technology Agency (JST), Kawaguchi, Saitama, Japan
[4]Department of Orthopedic Surgery, Keio University School of Medicine, Shinjuku, Tokyo, Japan
[5]Chugai Pharmaceutical Company Ltd., Tokyo, Japan
[6]Department of Medical Science I, School of Health and Sport Sciences, Osaka University, Suita, Osaka, Japan
[7]Department of Immunology, Graduate School of Frontier Biosciences Osaka University, Suita, Osaka, Japan

Endogenous neural stem/progenitor cells (NSPCs) have recently been shown to differentiate exclusively into astrocytes, the cells that are involved in glial scar formation after spinal cord injury (SCI). The microenvironment of the spinal cord, especially the inflammatory cytokines that dramatically increase in the acute phase at the injury site, is considered to be an important cause of inhibitory mechanism of neuronal differentiation following SCI. Interleukin-6 (IL-6), which has been demonstrated to induce NSPCs to undergo astrocytic differentiation selectively through the JAK/STAT pathway in vitro, has also been demonstrated to play a critical role as a proinflammatory cytokine and to be associated with secondary tissue damage in SCI. In this study, we assessed the efficacy of rat anti-mouse IL-6 receptor monoclonal antibody (MR16-1) in the treatment of acute SCI in mice. Immediately after contusive SCI with a modified NYU impactor, mice were intraperitoneally injected with a single dose of MR16-1 (100 μg/g body weight), the lesions were assessed histologically, and the functional recovery was evaluated. MR16-1 not only suppressed the astrocytic diffentiation-promoting effect of IL-6 signaling in vitro but inhibited the development of astrogliosis after SCI in vivo. MR16-1 also decreased the number of invading inflammatory cells and the severity of connective tissue scar formation. In addition, we observed significant functional recovery in the mice treated with MR16-1 compared with control mice. These findings suggest that neutralization of IL-6 signaling in the acute phase of SCI represents an attractive option for the treatment of SCI. © 2004 Wiley-Liss, Inc.

Key words: spinal cord injury; IL-6; glial scar; inflammation; neural stem/progenitor cells

© 2004 Wiley-Liss, Inc.

Recent studies have shown the existence of neural stem/progenitor cells (NSPCs) in adult mammalian spinal cord and have raised the possibility that the spinal cord has latent capacity for self-repair in response to injury or disease through the use of endogenous NSPCs (Horner et al., 2000; Bjorklund and Lindvall, 2000). After a spinal cord injury (SCI), however, these cells proliferate and migrate to the lesion site, where they differentiate exclusively into astrocytes, never into neurons, and are eventually associated with glial scar formation (Johansson et al., 1999; Takahashi et al., 2003). Glial scar tissue is considered a physical barrier and prevents axonal regeneration by producing axonal growth inhibitors, such as chondroitin sulfate proteoglycans (David and Lacroix, 2003). The major causes of this inhibitory mechanism of neuronal differentiation include the microenvironmental factors that dramatically change immediately following SCI. The interleukin (IL)-6 family of cytokines has been shown to play especially important roles in regulating the various biological responses through multichain receptor complexes-mediated signaling (for review see Taga and Kishimoto, 1997). The multichain receptor complexes, which include the ligand binging receptor (e.g., IL-6-

Contract grant sponsor: Japanese Ministry of Education, Sports and Culture; Contract grant sponsor: Human Frontier Science Program Organization; Contract grant sponsor: Core Research for Evolutional Science and Technology (CREST).

*Correspondence to: Hideyuki Okano, Department of Physiology Keio University School of Medicine, 35 Shinanomachi, Shinjuku, Tokyo, 160-8582, Japan. E-mail: hidokano@sc.itc.keio.ac.jp

Received 8 July 2003; Revised 14 October; Accepted 5 November

Published online 8 March 2004 in Wiley InterScience (www.interscience.wiley.com). DOI: 10.1002/jnr.20044

receptor) and nonligand binding membrane glycoprotein gp130 (Taga et al., 1989), have been shown to play essential roles in signal transduction of the IL-6 family of cytokines. Many lines of evidences suggest that this family of cytokines plays important roles in regulating the immune response (Taga and Kishimoto, 1997), inflammation, and central nervous system (CNS) development and significantly increases in the spinal cord after it is injured (Pan et al., 2002; Nakamura et al., 2003), and gp130-mediated signaling has been demonstrated to induce astrocytic differentiation of NSPCs through the JAK/STAT pathway in vitro (Bonni et al., 1997; Nakashima et al., 1999), suggesting the possibility that blockade of IL-6 trans-signaling after SCI may diminish the reactive astrogliosis and ameliorate functional recovery. Moreover, the IL-6 released during the acute phase of SCI promotes the inflammatory cell chemotaxis and is involved in the secondary injury cascade that is mediated by active inflammatory cell and molecular processes. A recent study has shown that excess activation of gp130 signaling by hyper-IL-6 (a bioactive IL-6/sIL-6R fusion protein) following SCI is associated with a robust inflammatory and glial response that appears to reduce axonal outgrowth in the adult mammalian CNS (Lacroix et al., 2003).

In this study, we used a murine SCI model to investigate the effects of blockade of IL-6 signaling with a monoclonal antibody against the IL-6 receptor (MR16-1, a rat monoclonal antibody that is known to bind to the mouse IL-6-receptor and block the Il-6-mediated cellular responses; Tamura et al., 1993; Takagi et al., 1998; Katsume et al., 2002; Okazaki et al., 2002). We examined whether MR16-1 treatment would offer the promise of a new therapeutic strategy for treating SCI. The results showed that MR16-1 suppressed not only the glial differentiation of NSPCs caused by IL-6 signaling in vitro but also the astrogliosis after SCI in vivo. MR16-1 also decreased infiltration by inflammatory cells and scar tissue formation at the lesion site. In addition, the MR16-1-treated mice showed significantly better functional recovery than the nontreated mice.

MATERIALS AND METHODS

Animals

In total, 74 adult female C57BL/6J mice (18–22 g, 8–10 weeks of age) were used for this study. The ethics committee of our institution approved all surgical interventions and animal care procedures, which were in accordance with the Laboratory Animal Welfare Act, the *Guide for the Care and Use of Laboratory Animals* (National Institutes of Health), and the Guidelines and Policies for Animal Surgery provided by the Animal Study Comittees of the Central Institute for Experimental Animals and of Keio University.

Rat Anti-Mouse IL-6 Receptor Monoclonal Antibody (MR16-1)

The rat anti-mouse IL-6 receptor monoclonal antibody, MR16-1, was prepared as described previously (Tamura et al., 1993). The isotype of this antibody was Ig-G1. MR16-1 was shown to bind to the soluble IL-6 receptor of the mouse and suppress IL-6-induced cellular responses in a dose-dependent fashion (Okazaki et al., 2002). Other basic characterizations of this antibody have been described in previously published reports (Tamura et al., 1993; Okazaki et al., 2002).

Primary Cultures and Passaging Procedures

Spinal cord tissue was dissected from adult mice and transferred into Hank's balanced salt solution (HBSS) containing trypsin (1.33 mg/ml), hyaluronidase (0.67 mg/ml), and kynurenic acid (0.2 mg/ml; all from Sigma, St. Louis, MO) and then minced. After digestion for 4 min at 37°C, the tissue was transferred to HBSS containing trypsin inhibitor (0.7 mg/ml; Roche Diagnostics, Mannheim, Germany) and DNase (0,01 mg/ml; Boehringer Mannheim, Indianapolis, IN). Cells and tissue fragments were washed once with DMEM containing 10% fetal bovine serum (FBS; Hyclone, Logan, UT) and dissociated with a 5-ml pipette. Whole digested tissue was washed again and suspended in DMEM-10% FBS, filtered through sterile 100-mm nylon mesh, and thoroughly mixed with an equal volume of Percoll solution. The cell suspension was fractionated by centrifugation for 30 min, 18°C at 12,300 rpm. Cell fractions were harvested and washed free of Percoll by three rinses in DMEM/10% FBS. After a final centrifugation, the cell suspension was harvested in standard neurosphere culture medium and propagated as described previously (Reynolds and Weiss, 1992; Shimazaki et al., 2001). After the neurosphere-like cell masses had grown to near-confluence, they were passaged and replated at a density of 2×10^5 cells/ml. For differentiation assay, spheres passaged five or six times were dissociated into single cells and plated onto poly-L-ornithine (PO)-coated coverslips at a density of 5×10^5 cells/ml. To investigate the effects of IL-6 signaling on the neural progenitors, we added both IL-6 and soluble IL-6 receptor to the culture medium. As reviewed by Van Wagoner and Benveniste (1999), unlike most soluble receptors that act as antagonists to their respective ligands, the soluble receptor of IL-6 has been shown to function as an agonist of the IL-6-mediated cellular responses by binding to the nonligand binding glycoprotein gp130 (Taga et al., 1989), which acts as a signal transducer of the IL-6 family of cytokines (Taga and Kishimoto, 1997). In the present study, the dissociated adult mouse spinal cord-derived neural precursor cells that had been prepared as described above, were allowed to differentiate for 3 days in the presence of IL-6 (20 ng/ml) and soluble IL-6 receptor-α (sIL-6R; 20 ng/ml), with or w/o MR16-1 (25 μg/ml).

Spinal Cord Injury Model

Female C57BL/6J mice were anesthetized with an intraperitoneal injection of ketamine (100 mg/kg) and xylazine (10 mg/kg). After laminectomy at the T9 level, the dorsal surface of dura matter was exposed. The vertebral column was stabilized with fine forceps and clamps at the T7 and T10 spinous processes and ligament, and the animal's body was then lifted. SCI was induced with a modified NYU impactor (Gruner, 1992; Kuhn and Wrathall, 1998; Jakeman et al., 2000). A 3-g weight (1.2-mm-diameter tip) was allowed to drop from a height of 25 mm onto the dorsal surface of the dura matter. The muscles and the incision were then closed in layers, and the

animals were placed in a temperature-controlled chamber until thermoregulation was reestablished. Manual bladder expression was performed twice per day until reflex bladder emptying was reestablished.

Injection of MR16-1 and BrdU

Immediately after the SCI, mice were intraperitoneally injected with a single dose of MR 16-1 (100 μg/g body weight; MR16-1 group) or with the same volume and concentration of purified rat IgG (ICN/Cappel Ohio; control group). To label the cells that divided after the injury, a sterile solution of bromodeoxyuridine (BrdU; 50 μg/g body weight; Sigma) was intraperitoneally injected daily for 2 weeks after the SCI.

Behavioral Analysis

Three different tests were used to assess recovery of motor function after SCI. We examined 30 injured mice (15 animals per group) for functional evaluation. Each mouse was tested at 1, 3, 5, and 7 days postoperatively and weekly thereafter until 6 weeks. Every test was performed in a double-blind fashion and recorded on videotape.

Open-field locomotion. Motor function of the hindlimbs was evaluated by the locomotor rating test on the Basso-Beattie-Bresnahan (BBB) scale, as described previously (Basso et al., 1996). A team of three experienced examiners evaluated each animal for 4 min and assigned an operationally defined score for each hindlimb.

SCANET. Motor function was evaluated with a SCANET automated motion-analysis system (MV-10, Toyo Sangyo Co., Ltd., Toyama, Japan) developed to measure spontaneous motor activity in small animals. SCANET consists of a cage equipped with two crossing sensor frames arranged at different heights that allow monitoring of small (M1) and large (M2) horizontal movements plus the vertical movement involved in rearing (RG). The M1 and M2 scores represent total distances moved, and the RG score represents the frequency of vertical movements within a certain period, which is useful for assessing recovery of limb function after SCI in mice, as reported previously (Mikami et al., 2002). Each mouse was individually placed in the SCANET cage, and its spontaneous locomotor activity was measured for 10 min.

Rota-rod treadmill. Motor coordination was assessed with a rotating rod apparatus (Muromachi Kikai Co., Ltd., Tokyo, Japan), consisting of a plastic rod (3 cm diameter, 8 cm long) with a gritted surface, flanked by two large discs (40 cm diameter). A mouse was placed on the rod, and the rod was rotated at speeds of 5, 10, and 15 rpm. Latency until a fall occurred was monitored for 120 sec (Ogura et al., 2001). Three trials were conducted at each speed, and the average and maximum numbers of seconds were recorded.

Immunohistochemistry

At 2 weeks after the SCI, animals in both the MR16-1 group and the control group were deeply anesthetized by inhalation of diethyl ether and transcardially perfused with 4% paraformaldehyde in 0.1 M phosphate-buffered saline (PBS) for histological studies. Spinal cord tissue was removed and post-fixed with 4% paraformaldehyde in PBS for a few hours at room temperature. Tissue samples were immersed in 10% sucrose in PBS at 4°C for 24 hr, placed in 30% sucrose in PBS for 48 hr, and embedded in OTC compound. The embedded tissue was immediately frozen in liquid nitrogen and stored at −80°C until needed. Frozen sections of spinal cord 20 μm thick were cut on a cryostat in the axial and sagittal plane and stained with hematoxylin and eosin. For the immunofluorescence double-labeling experiment, spinal cord sections were permeabilized with 0.03% Triton X-100 and 10% normal goat serum in 0.01 M PBS, pH 7.4, for 30 min. As primary antibodies, rat anti-BrdU 1:200 (Abcam, Cambridge, United Kingdom), rabbit anti-GFAP antibody 1:1000 (Dako, Carpinteria, CA), rat anti-Mac-1 1:200 (Pharmingen, San Diego, CA), or human anti-Hu 1:2,000 (a gift from Dr. Robert Darnell, The Rockefeller University) were applied to the sections at 4°C overnight. The sections were then incubated with secondary antibodies conjugated with Texas red, fluorescein isothiocyanate (FITC; all from Jackson Immunoresearch, West Grove, PA) for 1 hr at room temperature. The slides were then washed, wet mounted, and examined under a fluorescence microscope. For diaminobenzidine (DAB; Sigma) staining, rat anti-Mac-1 antibody 1:200 (Pharmingen) was used as the primary antibody, followed by a horseradish peroxidase (HRP)-labeled goat anti-rat IgG as the secondary antibody. Staining was visualized with DAB, and slides were washed, dehydrated, cleared in xylene, and mounted. For the in vitro study, cells cultured on chamber slides were fixed with 4% paraformaldehyde in PBS and subjected to immunofluorescence staining. Rabbit anti-GFAP antibody 1:1,000 (Dako) was used as the primary antibody, followed by FITC-conjugated goat anti-rabbit IgG as the secondary antibody. The cells were counterstained with Hoechst 33258 to identify nuclei.

Quantitative Analysis

Images were obtained by fluorescence microscopy (Axioskop 2 plus; Carl Zeiss Co., Ltd., Tokyo, Japan). For quantification of connective tissue scar (CTS) formation in vivo, five representative axial sections, 1.0 mm and 0.5 mm rostral to the lesion epicenter, at the lesion epicenter, and 0.5 mm and 1.0 mm caudal to the lesion epicenter were selected from a 4-mm length of cord, centered over the impact site, and the CTS area was measured using NIH Image software in H&E-stained sections and calculated as a percentage of the total axial area. To evaluate astrogliosis, five representative axial sections were selected as described above, and six regions in each section were captured randomly at ×200 magnification by confocal microscopy (LSM510; Carl Zeiss Co., Ltd.). The glial fibrillary acidic protein (GFAP)/BrdU double-positive cells in each region were counted by three investigators in a blinded fashion, and the density of each section (number of GFAP/BrdU double-positive cells per total axial area) was calculated. To quantify the proportion of the lesion that was Mac-1 immunolabeled, five representative midsagittal sections (3 mm long) were selected, and the immunoreactive area was measured with the MCID system (Imaging Research, Inc., Toronto, Ontario, Canada).

Western Blot Analysis

At 12 hr after the injury, spinal cord tissue of the lesion epicenter (6 mm long) was dissected from the mice (four animals per group and four sham-operated animals), homogenized in MAPK lysis buffer containing protease inhibitor, and after son-

ication centrifuged at 15,000 rpm. Protein from the supernatant of each sample was separated by 10% SDS-PAGE and transferred to polyvinylidene difluoride membranes by electrophoresis. The membranes were blocked for 1 hr at room temperature in TBST buffer containing 4% nonfat milk, NaCl (150 mM), and 0.05% Tween 20. The blots were then incubated with either primary polyclonal rabbit anti-stat3 antibody, rabbit antiphospho-stat3 antibody 1:500 (Cell Signaling Technology, Beverly, MA), mouse anti-α-tubulin antibody 1:500, or rabbit anti IL-6Rα antibody 1:200 (Santa Cruz Biotechonology, Santa Cruz, CA), followed by a secondary HRP-conjugated anti-rabbit or mouse IgG antibody. The blots were visualized with the ECL Blotting Analysis System (Amersham, Arlington Heights, IL).

Statistical Analysis

Values are reported as means ± SEM. Differences in all tests except for the rearing score analysis were analyzed for statistical significance by the unpaired Student's *t*-test. SCANET rearing scores were compared between groups by ANOVA with the post hoc Fisher's exact test. In all statistical analyses, significance was accepted at $P = .05$.

RESULTS

Effect of MR16-1 on Neural Stem/Progenitor Cells In Vitro

We investigated the effect of IL-6 signaling and MR16-1 on NSPC differentiation in vitro by performing the differentiation assay on adult spinal cord-derived neural precursor cells that had been expanded in a floating culture according to a previously reported method (Reynolds and Weiss, 1992; Shimazaki et al., 2001). Approximately 47.1% of the control NSPCs cultured in medium alone differentiated into astrocytes (Fig. 1A1,B). After addition of IL-6 and sIL-6R to induce gp130-mediated signaling (Taga et al., 1989; Tamura et al., 1993), NSPC differentiation into astrocytes was enhanced, and there was obvious extension of GFAP-positive processes (Fig. 1A2,B). By contrast, addition of MR16-1 to IL-6 plus sIL-6R inhibited the effect of IL-6 plus sIL-6R on astrocytic differentiation (Fig. 1A3), and there was a significant decrease in GFAP-positive cells as a percentage of total live cells in the MR16-1 group compared with the IL-6 plus sIL-6R-alone-treated group (mean value of 43.2% ± 2.8% in the MR16-1 group compared with 64.9% ± 3.5% in the IL-6 plus sIL-6R group; Fig. 1B). There was no significant difference in the number of total live cells between these two groups. These results indicate that the astrocytic differentiation-promoting effect of the IL-6 signal was sufficiently blocked by MR16-1 in vitro.

Histological Changes in Mice After SCI

Two weeks after the SCI, there was no cavitation at the lesion epicenter, but the central gray matter had been completely replaced by CTS in both the control group and the MR16-1 groups (Fig. 2). Single or double immunostaining was then performed to determine composition of the cells at the lesion site. Mac-1-positive inflammatory cells were observed mainly in the scar area (Fig. 2H,I), and Hu-positive neurons were found to remain only in the spared white matter (Fig. 2E,F) compared with uninjured mice (Fig. 2D,G). On the other hand, there were few GFAP-positive cells within the central lesion area, and it was surrounded by GFAP-positive astrocytes in both the axial and the sagittal sections (Fig. 3). We found that the area of the CTS was essentially GFAP negative. Interestingly, the CTS area was smaller in the MR16-1 group (Fig. 3B,D) than in the control group (Fig. 3A,C). Double immunostaining with GFAP and BrdU revealed BrdU in the nuclei of the GFAP-positive cells, indicating that they had divided after the SCI, and they were concluded to be reactive astrocytes.

To determine whether administration of MR16-1 suppressed astrogliosis after SCI, we counted the numbers of GFAP and BrdU double-positive cells at the epicenter and 0.5 and 1.0 mm rostral and caudal to the epicenter (Fig. 4). Representative confocal images of the lesioned area under higher magnification are shown in Figure 4A (control group) and 4B (MR16-1 group). In the MR16-1 group, there were significantly fewer GFAP and BrdU double-positive cells than in the control group (mean of 85.1 ± 2.5 cells/mm^2 in the control group compared with 63.3 ± 9.3 cells/mm^2 in the MR16-1 group; Fig. 4C).

Western Blotting

We confirmed the significantly increased expression of the IL-6 receptor in the injured spinal cord by Western blot analysis. In the intact spinal cord of sham-operated mice (in which only laminectomy was performed), the expression level of the IL-6 receptor was very low. However, the expression level had increased by nearly eightfold at 12 hr after the injury (Fig. 5A,C). To investigate whether the decrease in reactive astrocytes was due to blockade of the IL-6 signal cascade, we performed an analysis of both the total and the phosphorylated forms of the signal transducer and activator of transcription 3 (STAT3), a principal part of the IL-6 family signal cascade. Initiation of IL-6 signaling occurs when IL-6 binds to the IL-6R, which leads to association with gp130, and this receptor complex leads to activation of gp130-associated tyrosine kinases (JAK kinases). JAK activation then leads to tyrosine phosphorylation of STATs (Taga and Kishimoto, 1997; Van Wagoner and Benveniste, 1999; Ohtani et al., 2000). Upon phosphorylation, STAT3 proteins dimerize and translocate to the nucleus, where they bind to elements in the promoter of GFAP genes (Bonni et al., 1997), so quantification of phosphorylated STAT3 is an adequate index of the extent of IL-6 signaling. Administration of MR16-1 decreased the expression of phosphorylated STAT3 compared with the control group (Fig. 5B), and there was a significant difference in the ratio of phosphorylated to total STAT3 expression between the control group and the MR16-1 group (Fig. 5D). These findings suggested that the intraperitoneally injected MR16-1 actually blocked the IL-6/JAK/STAT3 signaling pathway and suppressed astrogliosis after SCI. However, strictly speaking, the alternative possibility that the observed reduction in the phosphorylated STAT3 level in the MR16-

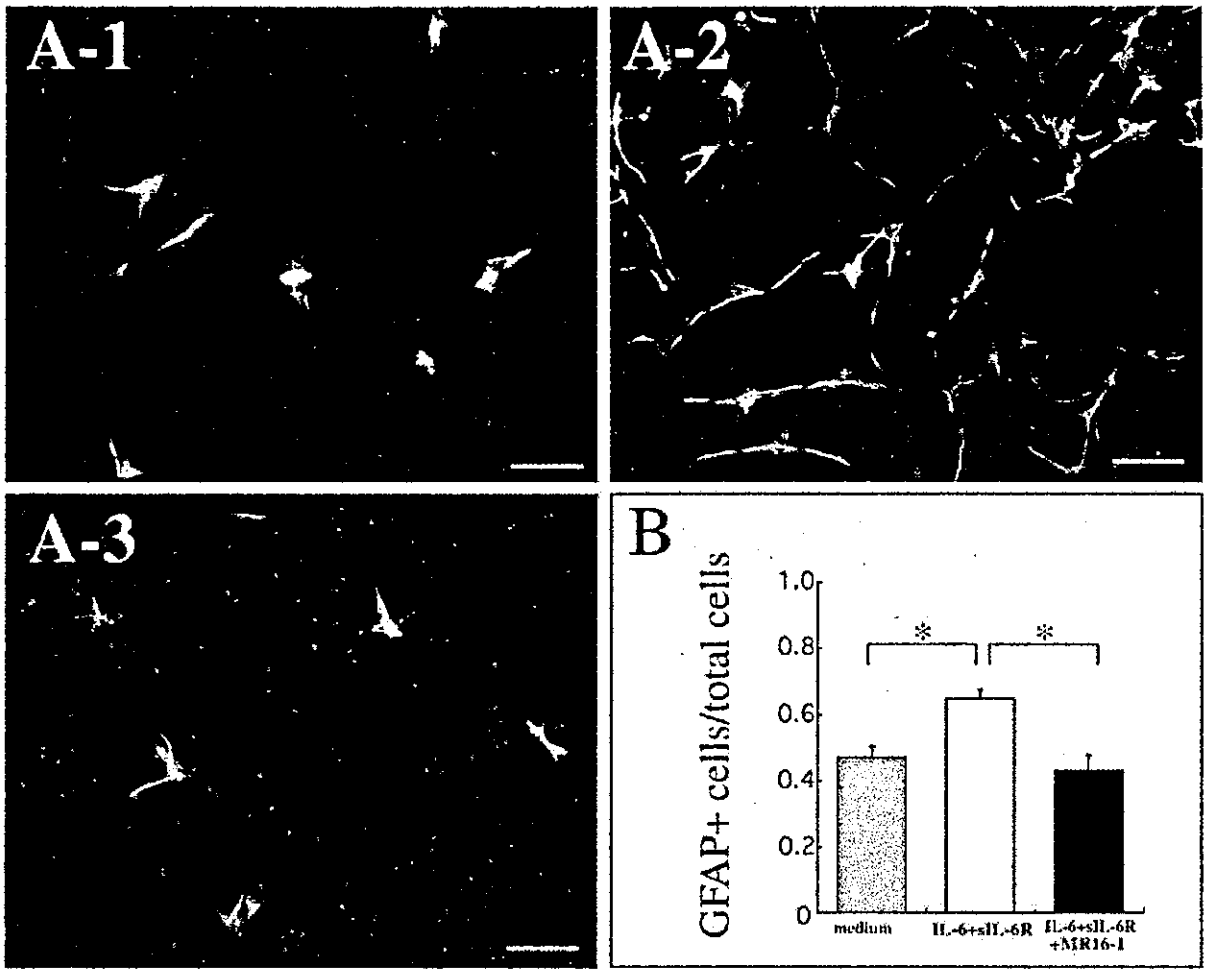

Fig. 1. Effect of the IL-6 signal and MR16-1 on the astrocytic differentiation of NSPCs. **A:** Dissociates of neural progenitor cells were cultured for 3 days with medium alone (A1), IL-6 and soluble IL-6 receptor at 20 ng/ml (A2), and IL-6 and soluble IL-6 receptor plus MR16-1 at 20 μg/ml (A3) and then subjected to immunofluorescence staining for GFAP (green) and Hoechst 33258 (blue). **B:** The number of GFAP-positive cells was calculated as a percentage of all live cells. Values are means ± SEM. $*P < .05$; two-tailed t-test ($n = 3$). Scale bars = 50 μm.

1-treated group resulted from suppression of astrogliosis by some unknown mechanisms cannot be excluded.

MR16-1 Suppressed the Infiltration by Inflammatory Cells After SCI

In addition to regulation of the astrocytic differentiation of NSPCs, IL-6 plays critical roles as a proinflammatory cytokine that activates macrophages and induces inflammatory cell chemotaxis and fibroblast proliferation (Romano et al., 1997; Van Wagoner and Benveniste, 1999; Tuna et al., 2001). To determine the antiinflammatory effect of MR16-1, we therefore performed immunolabeling of Mac-1-positive cells in sagittal sections at the lesion epicenter. Fewer Mac-1-positive cells were observed at the lesion epicenter 2 weeks after the injury in the MR16-1 group (Fig. 6A,B), and quantitative analysis showed statistically significant differences Mac-1-immunolabeled area in the MR-16 group and in the control group (mean of 5.6% ± 1.0% in the MR16-1 group, compared with 15.1% ± 1.2% in the control group; Fig. 6C). We also measured the area of the CTS after SCI using NIH Image software in H&E-stained serial sections and found that the area of the scar at the lesion epicenter 2 weeks after injury was significantly smaller in the MR16-1 mice (mean 47.4% ± 1.3% in the MR16-1 group compared with 64.5% ± 2.7% in the control group; Fig. 6D). These results indicate that administration of MR16-1 attenuated the inflammatory responses following injury in vivo.